MARTIN MARIETTA ENERGY SYSTEMS LIBRARIES
3 4456 0069289 1

ORNL/TM-10065

ornl

OAK RIDGE NATIONAL LABORATORY

MARTIN MARIETTA

Center for Neutron Research Project Status Report

C. D. West
R. T. Primm III
G. L. Copeland
F. C. Difilippo
J. C. Griess
W. R. Gambill
R. M. Moon
I. I. Siman-Tov

OAK RIDGE NATIONAL LABORATORY
CENTRAL RESEARCH LIBRARY
CIRCULATION SECTION
4500N ROOM 175
LIBRARY LOAN COPY
DO NOT TRANSFER TO ANOTHER PERSON
If you wish someone else to see this report, send in name with report and the library will arrange a loan.

OPERATED BY
MARTIN MARIETTA ENERGY SYSTEMS, INC.
FOR THE UNITED STATES
DEPARTMENT OF ENERGY

Printed in the United States of America. Available from
National Technical Information Service
U.S. Department of Commerce
5285 Port Royal Road, Springfield, Virginia 22161
NTIS price codes—Printed Copy: A05 Microfiche A01

This report was prepared as an account of work sponsored by an agency of the United States Government. Neither the United States Government nor any agency thereof, nor any of their employees, makes any warranty, express or implied, or assumes any legal liability or responsibility for the accuracy, completeness, or usefulness of any information, apparatus, product, or process disclosed, or represents that its use would not infringe privately owned rights. Reference herein to any specific commercial product, process, or service by trade name, trademark, manufacturer, or otherwise, does not necessarily constitute or imply its endorsement, recommendation, or favoring by the United States Government or any agency thereof. The views and opinions of authors expressed herein do not necessarily state or reflect those of the United States Government or any agency thereof.

ORNL/TM-10065

Engineering Technology Division

CENTER FOR NEUTRON RESEARCH PROJECT STATUS REPORT

C. D. West
Project Manager

R. T. Primm III
Report Coordinator

G. L. Copeland
F. C. Difilippo
J. C. Griess
W. R. Gambill
R. M. Moon
I. I. Siman-Tov

Date Published: September 1986

Prepared by the
OAK RIDGE NATIONAL LABORATORY
Oak Ridge, Tennessee 37831
operated by
MARTIN MARIETTA ENERGY SYSTEMS, INC.
for the
U.S. DEPARTMENT OF ENERGY
under Contract No. DE-AC05-84OR21400

MARTIN MARIETTA ENERGY SYSTEMS LIBRARIES
3 4456 0069289 1

CONTENTS

	Page
LIST OF FIGURES	v
LIST OF TABLES	vii
NOMENCLATURE	ix
ABSTRACT	1
1. OBJECTIVES, DESIGN CRITERIA, CONSTRAINTS, AND PROJECT OVERVIEW	2
2. RESEARCH REQUIREMENTS	12
2.1 Neutron-Scattering Facilities	12
2.2 Isotope Production	17
2.3 Materials Irradiation	17
2.4 Analytical Applications	18
2.5 Nuclear Physics	19
3. REACTOR PHYSICS	20
3.1 Introduction	20
3.2 Analytical Calculations That Define Reactor Materials	20
3.3 Cross-Section Sets	23
3.4 Neutronics Codes	24
3.5 Benchmarking of Codes and Libraries	24
3.6 Reference Core Design	26
4. THERMAL-HYDRAULIC DESIGN	44
4.1 Introduction	44
4.2 Coolant, Cladding, and Fuel Temperatures	44
4.3 Fuel Plate Deflection, Vibration, and Erosion	45
4.4 Critical Flow Velocity for Fuel Plates	45
4.5 Core Pressure Drop	46
4.6 The Incipient-Boiling Heat Flux (ϕ_{ib}) and the Critical Heat Flux (ϕ_c)	46
4.7 Coolant Pressure Level	47
4.8 Power Density Profile and Surface Area Density	47
4.9 Maximum Core Power Density	48
4.10 Core Thermal/Flow Analysis Code	48
4.11 Results for the Reference Core	48

	Page
5. CORROSION OF ALUMINUM FUEL PLATE CLADDING	52
5.1 Introduction	52
5.2 Background Corrosion Information	52
5.3 Test Plan	54
5.4 Summary	55
6. FUEL MATERIALS	56
7. COLD SOURCE FEASIBILITY STUDY	58
7.1 Cold Neutron-Scattering Cross Sections	58
7.2 Computational Studies of the CNRR Cold Source	58
7.3 Revised Thermal Energy Group Structure	63
8. PROGRAM PLAN	65
REFERENCES	68

LIST OF FIGURES

Figure		Page
1	The CNRR reference core	6
2	Side view of reference core	7
3	Unperturbed flux—reference core at 270 MW	10
4	Unperturbed thermal fluxes for three research reactors	10
5	Schematic of CNR irradiation and beam facilities	11
6	Spectral distributions of various beams from reactor producing peak thermal flux of 5×10^{19} neutrons$\cdot m^{-2} \cdot s^{-1}$	16
7	Combinations of power and power density which yield a peak thermal flux in the reflector of 10^{20} neutrons$\cdot m^{-2} \cdot s^{-1}$	22
8	One-dimensional spherical model used to collapse 123-group library	24
9	One-dimensional slab model used to collapse 27-group library	25
10	Possible fuel plate configurations in annular geometry	27
11	U-235 concentration as function of r and z for reference core	35
12	Radial distribution of thermal flux in reference core	38
13	Axial distribution of thermal flux in reference core	39
14	Radial distribution of epithermal flux in reference core	40
15	Radial distribution of fast flux in reference core	41
16	Radial distribution of epithermal/thermal flux ratio (reference core)	42
17	Radial distribution of fast/thermal flux ratio (reference core)	43
18	Dependence of critical channel diameter on pressure for H_2O	47
19	Dependence of the ratio of critical to incipient-boiling heat fluxes on pressures	47
20	Parametric incipient-boiling depiction for D_2O at P = 6.9 MPa	49
21	Comparison of two oxide-thickness correlations	54

Figure		Page
22	Currently available silicide fuel irradiation data and expected CNR operating limits	57
23	Computer models used to investigate cold source	61
24	Neutron spectra at center of cold source	62
25	CNR program schedule	66

LIST OF TABLES

Table		Page
1	Major design criteria for the CNRR	3
2	Comparison of core characteristics	8
3	CNRR reference core design and project objectives	9
4	Distribution of instruments	12
5	Characteristic values of K for guide materials	14
6	Power (P) to produce a 10^{20} neutrons$\cdot m^{-2} \cdot s^{-1}$ thermal flux	21
7	Benchmarking of ILL and HFIR cores with the VENTURE system	26
8	Optimal dimensions for a bare cylindrical reactor	30
9	Fuel distribution for reference core	33
10	CNRR performance over a fuel cycle	43
11	Reference core: thermal and flow parameters I	50
12	Reference core: thermal and flow parameters II	50
13	Reference core: thermal and flow parameters III	51
14	Comparison of ILL and CNR cold sources	59
15	Distribution function for neutrons in thermal equilibrium with a cold source at 20 K	63
16	Thermal energy boundaries for future cold source calculations	64
17	Financial plan for CNR experiments and development tests	65

NOMENCLATURE

Notation

D	diameter
MF	metal fraction
P	pressure
ΔP	pressure drop
Q	coolant volumetric flow rate
q'''	power density
t	temperature
Δt_{sub}	coolant subcooling ($t_{sat} - t_b$)
V	coolant velocity
pt	plate thickness
δ	thickness
ε	mean roughness-element height
θ	time
ρ	fluid density
σ	surface tension
ϕ	heat flux

Subscripts:

b	bulk coolant
bl	boundary layer
c	critical
e	equivalent
HS	hot spot
i	core inlet
ib	incipient boiling
l	liquid
o	core outlet
ox	oxide
sat	saturation
syst	primary system
v	vapor

CENTER FOR NEUTRON RESEARCH PROJECT
STATUS REPORT

C. D. West
Project Manager

R. T. Primm III
Report Coordinator

G. L. Copeland
F. C. Difilippo
J. C. Griess
W. R. Gambill
R. M. Moon
I. I. Siman-Tov

ABSTRACT

The Center for Neutron Research (CNR) will provide the world's best facilities for the study of neutron scattering. The CNR will contain a very high flux reactor that will achieve an extremely high power density (between 4 and 8 MW/L). The reactor is to be fueled with uranium silicide and cooled, moderated, and reflected by D_2O. Initial reactor physics calculations indicate that a power level of 270 MW with a reactor core volume of 35 L will achieve a peak thermal flux in the reflector of 10^{20} neutrons$\cdot m^{-2} \cdot s^{-1}$. The reactor fuel will be contained in thin (1.3-mm) plates, similar to those employed in the very successful High-Flux Isotope Reactor, and will be graded in the axial and radial directions. Coolant velocity is to be 27 m/s, and core inlet pressure is to be 5.6 MPa. Maximum fuel centerline temperature will be ~350°C.

Initial thermal-hydraulic studies indicate that some method of preventing the formation of aluminum oxide on the fuel clad is required if the highest performance is to be achieved. Tests to confirm these calculations are planned.

One of the experimental facilities is to be a cold (10-meV) neutron source. Calculations to determine the size of the source have been initiated, but additional cross-section data are needed.

An abbreviated version of a tentative program plan for fiscal year 1987 and beyond is described. Total program expenditures are expected to be $40 million over 5 years.

1. OBJECTIVES, DESIGN CRITERIA, CONSTRAINTS, AND PROJECT OVERVIEW

C. D. West

The formal objectives of the Center for Neutron Research (CNR) project are to:

1. design and construct the world's best research reactor for neutron scattering;
2. provide isotope production facilities that are as good as, or better than, the High-Flux Isotope Reactor (HFIR);
3. provide materials irradiation facilities that are as good as, or better than, HFIR.

To guide the design work more easily, these objectives have been translated into quantitative design criteria against which proposed reactor core designs and concepts can be measured.

For neutron scattering, the main user requirements are a high thermal neutron flux, established over a sufficiently large volume to accommodate a number of beam tubes, one or more cold neutron (energy $\sim 10^{-4}$-eV) sources, and a hot neutron (energy ~0.3-eV) source. The thermal flux should be as free as possible of epithermal and fast neutrons.

The obvious comparison for a high-flux neutron-scattering source is the Institut Laue-Langevin (ILL) reactor: ILL is currently the world's leading center for neutron-scattering research. The design criteria for the CNR reactor (CNRR), based upon a comparison with existing facilities and the user requirements expressed to and established by the Seitz-Eastman Committee of the National Academy,[1] are shown in Table 1. The most significant single number is the peak thermal flux in the reflector, 5 to 10×10^{19} neutrons$\cdot m^{-2} \cdot s^{-1}$; for comparison, the ILL and HFIR have a peak reflector thermal flux of "only" about 1.5×10^{19} neutrons$\cdot m^{-2} \cdot s^{-1}$. Furthermore, the HFIR has a beryllium reflector that results in a much narrower peak in the thermal flux and, therefore, a much smaller volume of high flux than occurs in the heavy-water reflector at ILL.

The requirements for instruments, beam tubes, beam guides, and cold source(s) associated with neutron scattering have been established in a number of workshops and meetings.[2-4]

Table 1. Major design criteria for the CNR

Field/quantity	Design criterion
Neutron scattering	
Peak thermal flux in reflector	$>5 \times 10^{19}$ $m^{-2} \cdot s^{-1}$
Thermal/fast flux ratio at beam tube mouths	>80
Thermal flux at cold source position	$>2 \times 10^{19}$ $m^{-2} \cdot s^{-1}$
Number of thermal and hot neutron beam tubes	16
Number of cold neutron guide tubes	8
Transuranium isotopes	
Epithermal flux at irradiation position	$\geq 0.6 \times 10^{19}$ $m^{-2} \cdot s^{-1}$
Epithermal/thermal flux ratio	≥0.25
Number of positions	≥20
Available diameter of position	16.6 mm
Available length of position	889 mm
Other isotopes	
Thermal flux at irradiation position	$\geq 1.7 \times 10^{19}$ $m^{-2} \cdot s^{-1}$
Number of positions	≥4
Diameter of positions	≥37 mm
Engineering materials irradiation (compared with HFIR target region)	
Fast flux	$\geq 1.4 \times 10^{19}$ $m^{-2} \cdot s^{-1}$
Fast/thermal flux ratio	≥0.5
Number of positions	≥6
Available diameter of positions	≥16.6 mm
Engineering materials irradiation (compared with HFIR removable beryllium positions)	
Fast flux	$\geq 0.5 \times 10^{19}$ $m^{-2} \cdot s^{-1}$
Fast/thermal flux ratio	≥0.3
Number of positions	≥8
Available diameter of positions	≥48 mm

For isotope production, high fluxes of neutrons are required with energies in the thermal or epithermal range. A substantial volume of space in regions of suitable flux is required to house the number of irradiation positions needed to match the facilities currently available at the HFIR. The production of transuranium isotopes requires facilities for processing the irradiated material. Such facilities and their equipment are specialized and expensive. Therefore, in the design of the

CNRR, an effort will be made to accommodate the standard irradiation capsule design that is used at the HFIR and processed in the existing facilities at Oak Ridge National Laboratory's (ORNL's) Transuranium Processing Facility (TRU). These requirements are included in Table 1.

Most experimenters who study the effects of radiation on engineering materials want a high flux that is very rich in fast neutrons, because the fast neutrons cause most of the property changes observed in irradiated materials. For certain experiments, particularly those relating to the magnetic fusion program, a low thermal flux or the possibility of locally reducing the thermal flux with shielding is important to the accurate simulation of the actual service conditions expected in real reactors. These requirements are also included in the design criteria (Table 1).

Table 1 represents an important step for the project; although subject to refinement and extension, quantitative criteria have been developed against which proposed core designs and changes to proposed designs can be measured.

In addition to the user needs expressed in the various publications already mentioned and incorporated in Table 1, the ORNL project management has imposed some important constraints on the reactor designers. One is the desire for a high availability of the reactor — the normal availability (the percentage of all time for which the reactor is operating) should be 80 to 85%. This value is comfortably between the figures for normal operation at ILL (70 to 80%) and at HFIR (90 to 95%). Refueling shutdowns are the major contributor to research reactor downtime and are almost inevitably longer for a heavy-water-cooled and -moderated reactor than for a light-water-cooled beryllium-moderated device because of the practical and safety problems associated with D_2O containing tritium. Until a detailed design and plan for refueling operations are available, no exact figure for the shutdown time is available. However, estimating that 2 to 3 d would not be an unreasonable figure means that the fuel element must last at least 2 weeks before replacement if the desired availability is to be achieved. The decision to aim for a 14-d fuel cycle length is important because it is one factor that determines both

the fuel load and the average fuel density of a reactor core of given size and power.

A second constraint, also with far-reaching consequences, is that the CNRR design must not *rely on* major technical advances, but the design should be one that can benefit from such advances if research provides them. Specifically, the design will call for the use of a fuel for which fabrication techniques and irradiation properties are well-known. Simultaneously, the project will call for the development of techniques to increase the permissible power density and provide for a core that would give a higher flux and acceptable life if higher power density fuel becomes available.

A reference core design has been evolved that, according to calculations based on a simplified model, meets or exceeds the design criteria of Table 1 within the constraints already described.

The reference core design provides some assurance that the objectives of the project can be met, as well as serving as a baseline against which improvements can be judged and a means for identifying needed research and development (R&D) (Fig. 1). The design is based on the aluminum-clad fuel plate design used by the HFIR. The fuel is in the form of one of the silicides (U_3Si_2) developed by Argonne National Laboratory for the Reduced Enrichment for Research and Test Reactors (RERTR) program. The silicides contain much more uranium than the same volume of the oxide fuel form used in HFIR. The uranium is highly enriched (93 wt % U-235) to minimize reactor volume, while meeting required cycle length and fluxes at minimum power.

The reference core design, then, involves 35 vol % U_3Si_2 with uranium enriched to 93% U-235 in an aluminum-clad aluminum matrix. The fuel loading is graded axially and radially, and the fuel plates are essentially the same size as the HFIR fuel plates. The reactor is cooled, reflected, and moderated by heavy water. The design has been carried through for two cases. In the base case, no significant technical advance over the HFIR and RERTR fuel technology is assumed. The core, with an active volume of 35 L (Fig. 2), is operated at 135 MW and the peak unperturbed thermal flux in the reflector is 5×10^{19} neutrons$\cdot m^{-2} \cdot s^{-1}$.

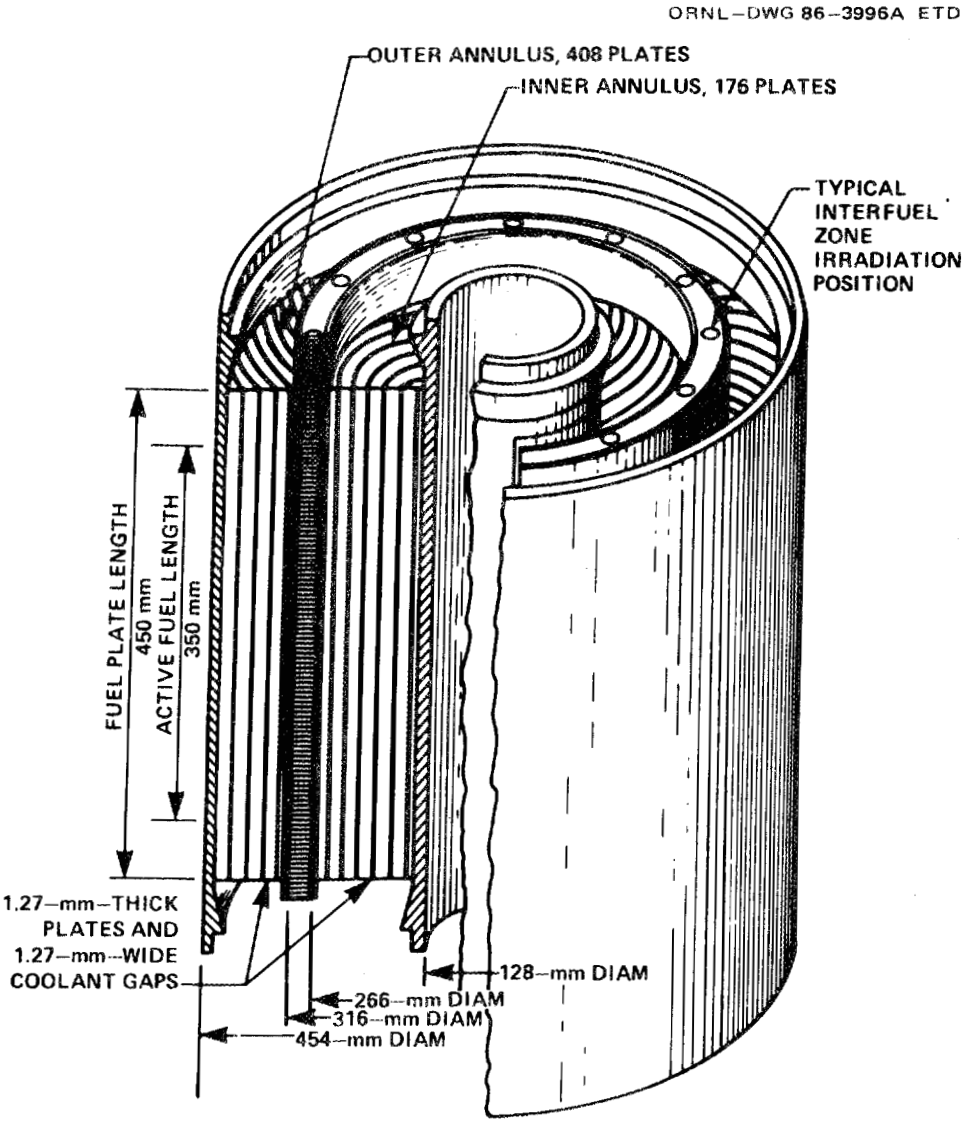

Fig. 1. The CNR reference core.

The limiting factor is the temperature rise across the layer of low-conductivity oxide (boehmite) that forms on the heated aluminum fuel cladding. A second case, chosen to show the extent to which the design can benefit from technical advances, assumes that a 90% reduction in the oxide formation rate can be achieved, perhaps by surface treatment, improvements in water chemistry, or choice of a more corrosion-resistant alloy for the cladding. In that case, the reactor power could be raised to 270 MW and the peak thermal flux would be 10^{20} neutrons$\cdot m^{-2} \cdot s^{-1}$. The

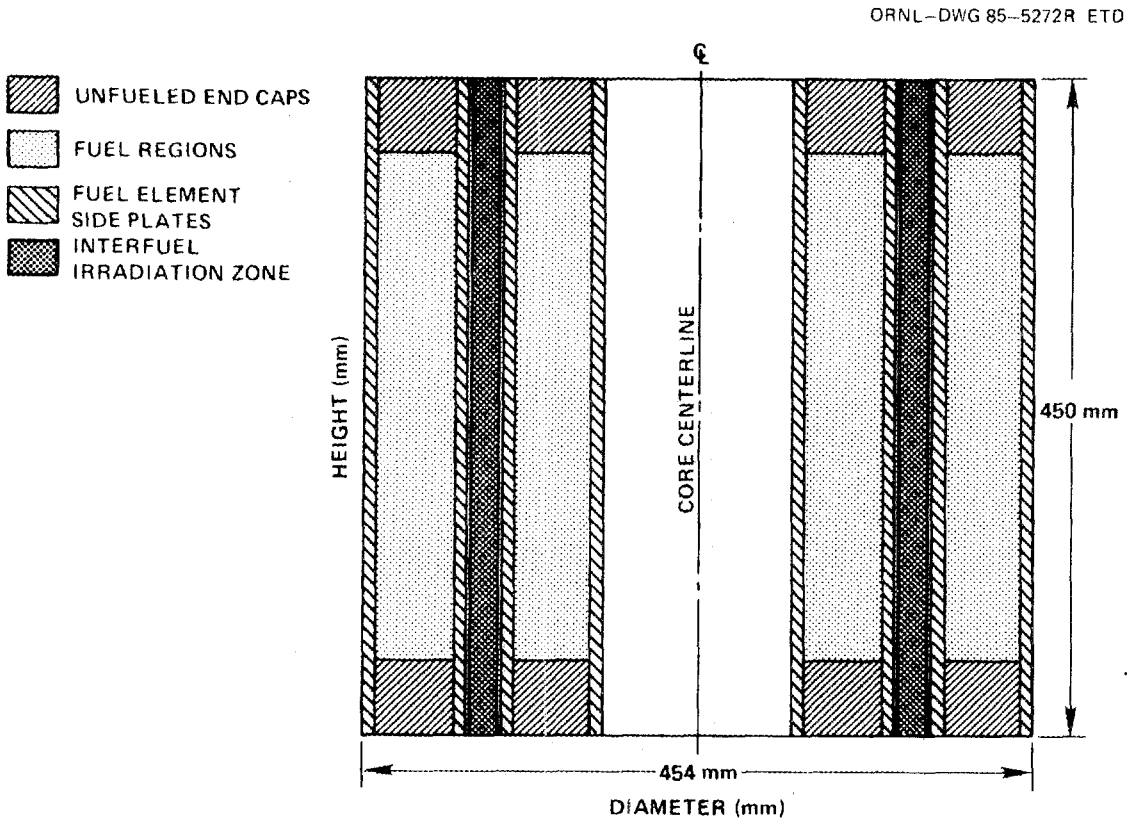

Fig. 2. Side view of reference core.

flux distribution is shown in Fig. 3. The major characteristics of the reactor are listed in Tables 2 and 3. That the design meets or exceeds the criteria established above is shown in Table 3. Figure 4 presents the calculated thermal flux distribution compared with HFIR and ILL. Figure 5 shows the relative locations of beam tubes, cold and hot sources, and irradiation positions. If the hot source is indeed located as indicated, three beam tubes would be aligned to receive neutrons from it.

Subsequent sections of this report relate the detailed considerations on which these data are based.

Table 2. Comparison of core characteristics

	HFIR	CNR reference core
Fuel form	U_3O_8	U_3Si_2
Matrix	Al	Al
Cladding	Al	Al
Coolant	H_2O	D_2O
Reflector/moderator	Be	D_2O
Fuel plate thickness, mm	1.27	1.27
Cladding thickness, mm	0.25	0.25
Coolant gap, mm	1.27	1.27
Inner fuel annulus[a]		
Inner diameter, mm	128.7	128.6
Outer diameter, mm	269.0	266.6
Outer fuel annulus[a]		
Inner diameter, mm	285.8	316.6
Outer diameter, mm	435.2	453.4
Fueled length, mm	508.0	350.0
Total core length, mm	609.6	450.0
Active volume, L	54.5	35.0
Coolant velocity, m/s	16	27
Inlet pressure, MPa	4.4	5.5
Outlet pressure, MPa	3.7	4.1
Inlet temperature, °C	49	50
Outlet temperature, °C	91	71[b]
Fuel loading, kg	9.4	18.1
Reactor power		
Baseline, MW	100	135
Enhanced, MW		270

[a]Including 7-mm side plates.

[b]71°C at 135 MW, 92°C at 270 MW.

Table 3. CNR reference core design and project objectives

Quantity	Design criterion	CNR	
		Reference[a]	Enhanced[b]
Core			
Power		135	270
Average core power density, MW/L	3.8[a]–8.6[b]	3.8	7.6
Fuel cycle length, weeks	>2	3[c]	2
End of beam tube			
Thermal flux, 10^{19} $m^{-2} \cdot s^{-1}$	5–10	5	10
Thermal/fast ratio	>80	100	100
Irradiation positions			
Fast flux,[d] 10^{19} $m^{-2} \cdot s^{-1}$	>1.4	3.9	7.9
Fast/thermal ratio[d]	>0.4	50	50
Epithermal flux,[e] 10^{19} $m^{-2} \cdot s^{-1}$	>0.6	1.6	3.1
Epithermal/thermal ratio[e]	>0.25	0.5	0.5
Thermal flux,[f] 10^{19} $m^{-2} \cdot s^{-1}$	>1.7	5	10

[a]With 15-d accumulation of oxide.

[b]With no oxide accumulation.

[c]Maximum: fuel would be changed after 15 d to limit oxide buildup.

[d]Interfuel positions.

[e]At epithermal peak in reflector.

[f]At thermal peak in reflector.

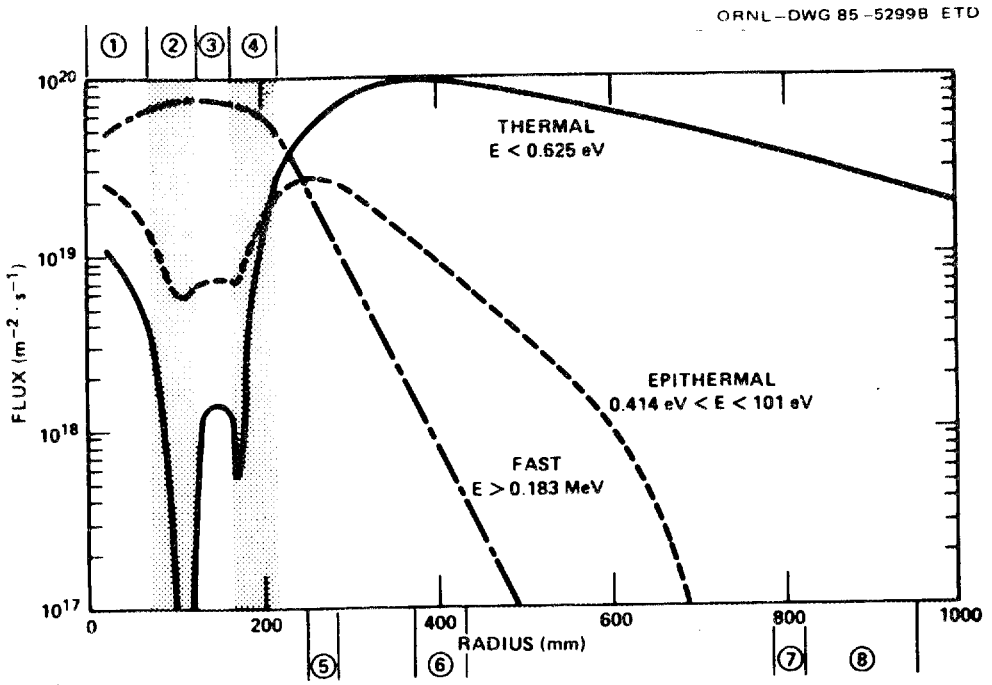

Fig. 3. Unperturbed flux—reference core at 270 MW.

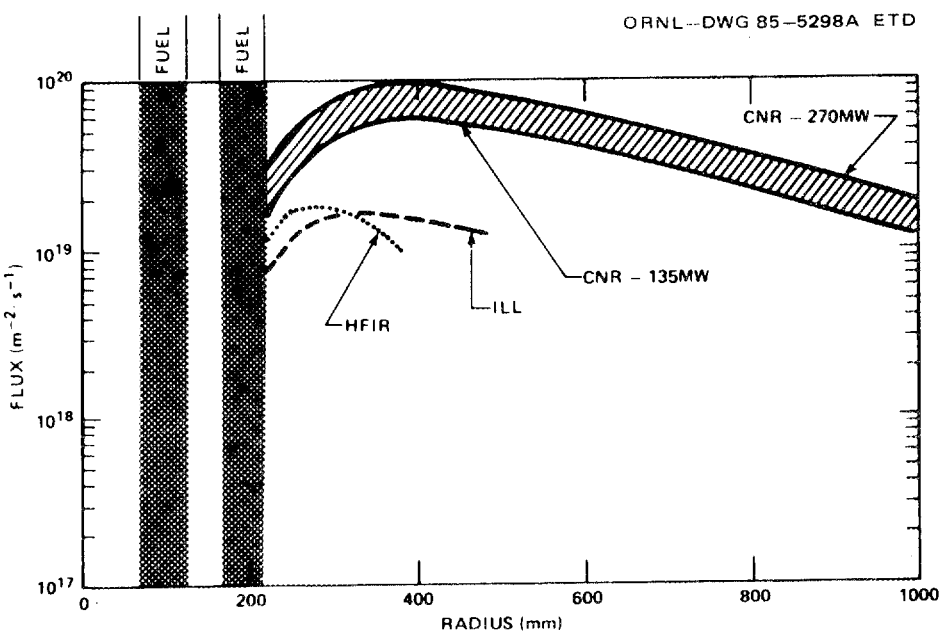

Fig. 4. Unperturbed thermal fluxes for three research reactors.

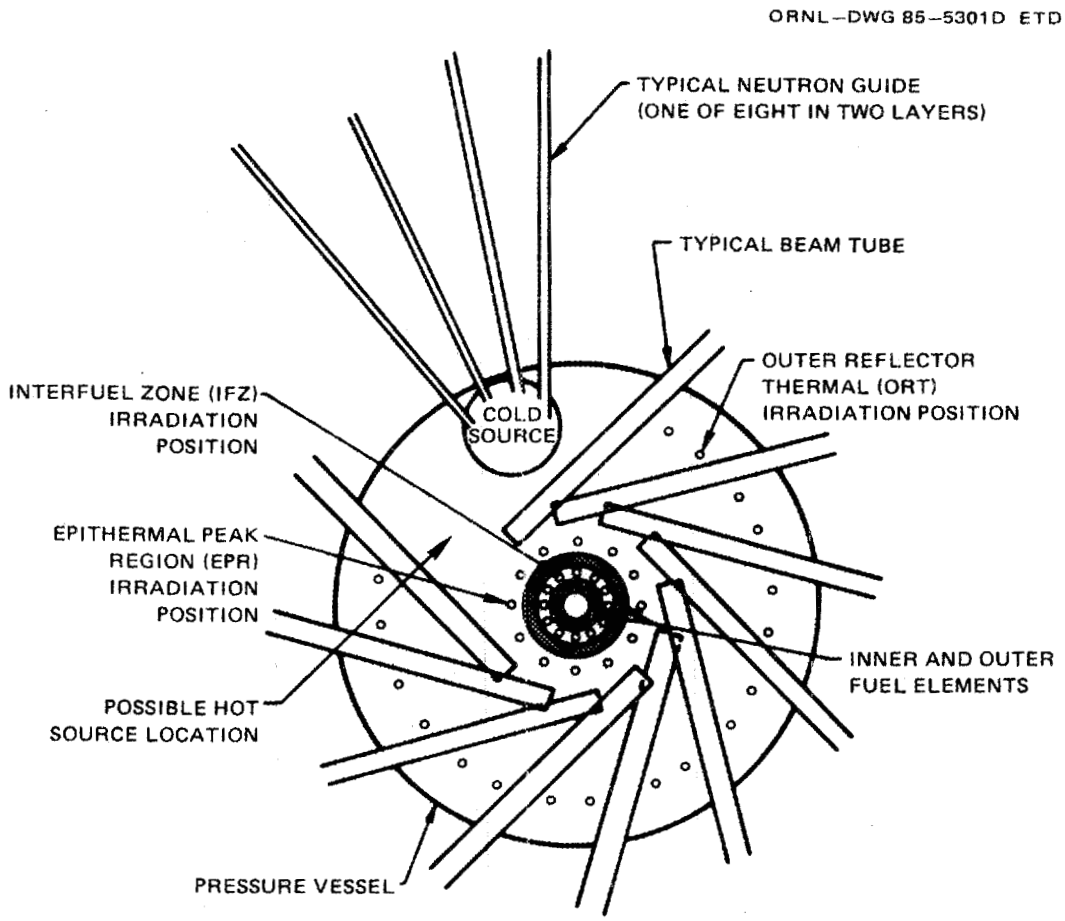

Fig. 5. Schematic of CNR irradiation and beam facilities.

2. RESEARCH REQUIREMENTS

R. M. Moon C. D. West

2.1 Neutron-Scattering Facilities

2.1.1 General remarks

Building a new reactor of unprecedented flux is only part of the CNR plan. Of equal importance is the task of constructing a variety of specialized neutron-scattering instruments, each carefully optimized to produce maximum counting rates. This task will require work on all instrument components: beam tubes, guides, collimators, monochromators, and detectors, as well as cold and hot sources to shift the thermal spectrum to lower or higher energies.

Initial plans call for eight cold guides to deliver neutrons to a large guide hall, ten horizontal beam tubes (eight thermal and two hot), and six slant tubes (two cold, three thermal, one hot) to provide experimental facilities on the second floor of the reactor building.

A first step in reaching a consensus on the types of instruments to include was taken at an ORNL workshop in May 1984. Summaries of discussions and recommendations for specific instruments are contained in the proceedings of this workshop.[5] The discussions covered the fields of solid state physics, chemistry, polymer science, biology, materials science, neutron optics, and nuclear physics. The highest priority was given to a total of 39 instruments, distributed as shown in Table 4, among

Table 4. Distribution of instruments

Beam type	Workshop recommendation	CNR plan
Cold	19	26
Thermal	16	11
Hot	4	3

cold, thermal, and hot beams. Table 4 also shows the number of instruments that can be accommodated with our tentative beam line plan, assuming three instruments per guide and one for each beam tube. Apparently, some consideration should be given to providing more thermal beams.

2.1.2 Beam tubes and guides

To a good approximation the neutron flux delivered to the outer end of a straight, nonreflecting tube is given by

$$I(\lambda) = \phi''(\lambda)\,\frac{A_s}{L_o^2} = \phi''(\lambda)\delta_H\delta_V \text{ [neutrons cm}^{-2}\text{ s}^{-1}\text{ Å}^{-1}\text{]} , \qquad (2.1)$$

where A_s is the cross-sectional area of the tube at the source end, L_o is the length of the tube, and $\phi''(\lambda)$ is the source flux per steradian and per wavelength interval. It is convenient to divide the solid angle factor (A_s/L_o^2) into horizontal and vertical angular divergences (δ_H and δ_V) because for many neutron-scattering instruments the resolution is strongly dependent on δ_H and almost independent of δ_V. For these cases, counting rates can be increased with no loss of resolution by increasing the vertical divergence. This immediately suggests the use of rectangular or elliptical beam tubes rather than circular tubes. The new JRR-3 reactor at Japanese Atomic Energy Research Institute will have rectangular beam tubes (60 by 100 mm) and the NRU reactor at Chalk River has elliptical tubes (98 by 225 mm). The present generation of high-flux reactors (HFIR, HFBR, and ILL) was built with circular tubes of about 100-mm diam, although some of the ILL tubes may have been altered. With source-to-monochromator distances of 5 to 7 m, this gives typical horizontal and vertical divergences of about 1°. For many applications, the vertical divergence could be doubled with no adverse effects and yield a gain of two in the number of useful neutrons. For high-resolution work, the horizontal divergence of ~1° is excessive. Reduction of the horizontal divergence may be achieved by providing Soller-slit collimators of selected divergence in the premonochromator flight path. In the initial planning for the CNRR, elliptical or rectangular tubes of dimensions 100 by 150 mm have been considered. A section of the flight path allowing selection of 3 to 4 different horizontal divergences is essential.

A beam guide is conceptually similar to a beam tube except that the interior walls have been specially prepared (very smooth) for total reflection of neutrons. Below some critical angle Θ_c, which depends linearly on the neutron wavelength and on the square root of the average coherent scattering amplitude of the surface material of the guide, neutrons will be totally reflected at the guide surface. The horizontal and vertical divergences of neutrons transmitted through a guide by total reflection are both $2\Theta_c$, so that the total flux transmitted by this mechanism is

$$I_R(\lambda) = \phi''(\lambda)\ 4\Theta_c^2\ (\lambda)\ . \tag{2.2}$$

In addition, a directly transmitted component will be determined by the guide geometry as in Eq. (2.1). The critical angle is given by

$$\Theta_c(\lambda) = K\ \lambda\ , \tag{2.3}$$

where the constant K is given in Table 5 for various guide surfaces. Supermirrors have not yet been used as guide coatings but should be considered for future applications. Supermirrors were developed at the ILL[6] as polarizing devices and have also been under development in Japan. They are made by evaporating successive, but nonperiodic, layers of at least two different materials. Further supermirror development is an appropriate area for R&D associated with the CNR. Supermirror guides would be particularly useful for transporting neutrons in the 1- to 3-Å range. However, the ultimate use of the neutrons must be kept in mind; it makes

Table 5. Characteristic values of K for guide materials

Material	K (radians $Å^{-1}$)
Ni	1.73×10^{-3}
^{58}Ni	2.05×10^{-3}
Supermirror	$\sim 3.81 \times 10^{-3}$

no sense to expend great effort to build a guide to transport neutrons of 4° divergence if the experimental requirement calls for 1° divergence. As an example, a normal nickel guide would transmit 5-Å neutrons over an angular range of 1°, while a supermirror guide would transmit 5-Å neutrons over an angular range of 2.2°.

Another area where an R&D program may be indicated is in the reflectivity of guide surfaces. According to P. Ageron[7] the actual H-15 guide transmission at the ILL is below the ideal transmission by a factor of two over a 60-m length.

For a long guide, the directly transmitted beam (including fast neutrons and γ-rays) can be eliminated by curving the guide. This has the very real advantage of reducing unwanted background in the guide hall. A curved guide acts like a band pass filter, cutting off short wavelengths (higher energies). The cut-off wavelength is given by

$$\lambda^* = \frac{1}{K} \sqrt{2d/\rho} \ , \tag{2.4}$$

where K is defined by Eq. (2.3), d is the guide width, and ρ is the radius of curvature. The disadvantage of curved guides is their lower transmission as illustrated in curves 4–8 in Fig. 6. The curved guide transmissions were calculated using formulas by Maier-Leibnitz and Springer.[8] For many applications, the reduction of short-wavelength neutrons is an advantage. For example, most crystal monochromators set to reflect wavelength λ will also reflect λ/2, λ/3, etc. A curved guide can help to reduce these unwanted higher-order contaminants.

2.1.3 Design issues

This general discussion is concluded by listing some of the fundamental design issues related to beam tubes and guides. As already indicated, tentative decisions have been reached on some of these questions:

1. number and shape of beam tubes — rectangular or elliptical,
2. standard beam tubes or shapes tailored to specific experiments,
3. number and shape of beam guides,
4. selection of radii of curvature for guides, and
5. selection of guide surface material.

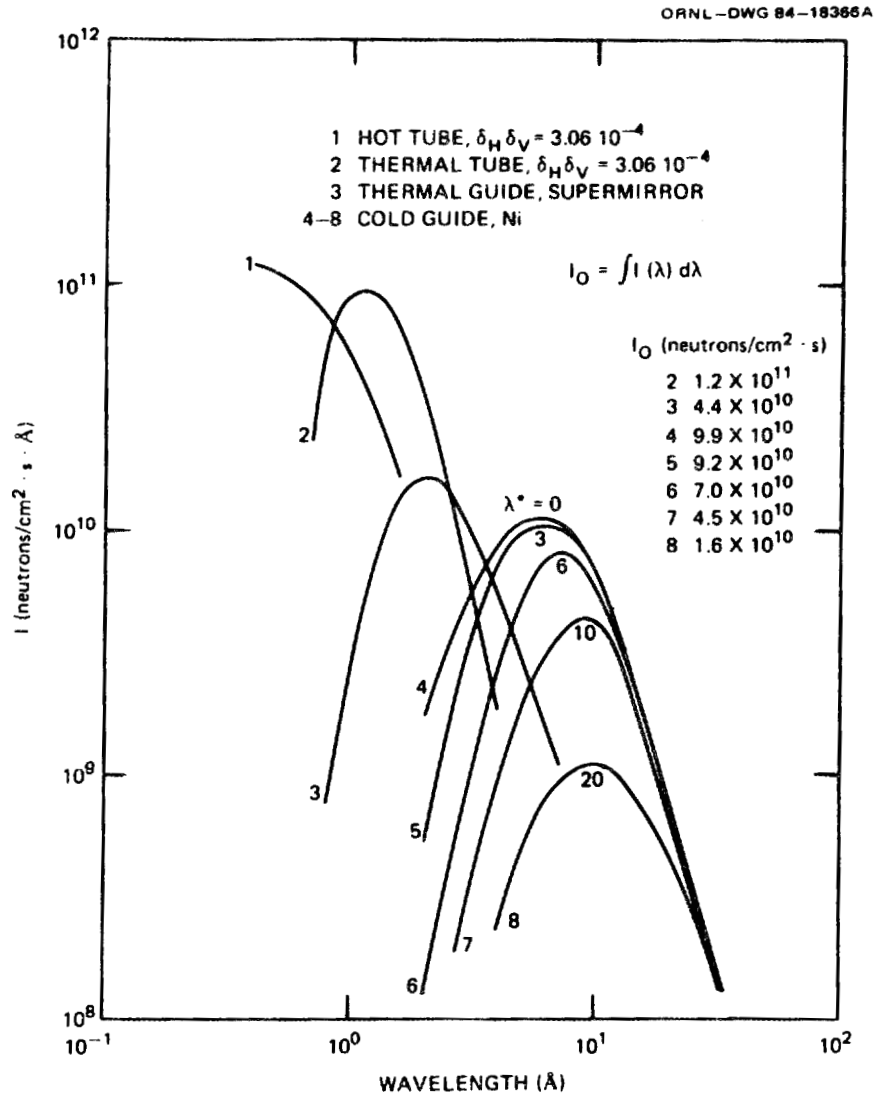

Fig. 6. Spectral distributions of various beams from reactor producing peak thermal flux of 5×10^{19} neutrons$\cdot m^{-2} \cdot s^{-1}$.

The proper selection of cross-sectional shapes of tubes and guides can not be made without considering the anticipated experimental uses. The expected widespread use of vertically focusing monochromator systems and the resulting impact on beam tube dimensions will be discussed in a future progress report.

2.2 Isotope Production

Most of the isotopes produced at ORNL come from the HFIR. The transuranium isotopes, for whose production the HFIR was specifically designed, are mainly produced in the target region, that is, the region inside the inner fuel element annulus. The precursor material is encapsulated in target rods of 16-mm diam and 889-mm length. The preirradiation and postirradiation processing of these capsules is undertaken with specially developed and highly specialized equipment at the TRU facility.

There are 30 isotope irradiation positions in the target region, but in recent years only 15 to 20 have typically been used for this purpose at any one time. The remainder are occupied by engineering materials irradiation capsules or are unused.

Most of the transuranium production irradiations require a high epithermal flux and a high ratio of epithermal-to-thermal flux. However, some specialized campaigns call for a pre-irradiation in a high thermal flux region. Other isotopes (mainly gadolinium-153, indium-192, and cobalt-60) are best produced in the highest thermal flux available, and with a high thermal-to-fast flux ratio. No estimates of the space, flux, and spectrum actually needed for production of isotopes other than the transuranium ones are available, nor is any estimate of the tradeoffs between available flux and needed space. However, a proposal has been received that calls for all of the space in the reflector not taken up by neutron-scattering facilities to be available for isotope production facilities if the neutronics are not affected adversely.

2.3 Materials Irradiation

Most of the materials irradiation experiments at ORNL are now carried out in the HFIR. The main requirement in experiments studying damage effects is for a high fast flux. The HFIR is currently being modified to provide better facilities for such experiments, and the CNRR must match the capabilities of the HFIR not as it is now, but as it will be following those modifications.

The fusion materials program, in attempting to simulate radiation damage effects in the first wall of a fusion device, requires a very hard spectrum if a realistic ratio of damage to transmutation effects is to be attained. There are techniques (such as tailoring the isotopic composition of the specimens) to provide useful results even from a mixed spectrum; however, a reactor with a range of available spectra would be preferred.

The highest fast flux in the HFIR is found in the target region, and space there is shared between the transuranium isotope production program (the major users) and materials irradiation experiments. The available positions are small, and the very high gamma heating rate in the target region also limits the size of the specimens that can usefully be irradiated there. At present, there is no access to the target region in HFIR for instrumentation, but the modification program will provide capability for two instrumented positions in the target. The interfuel zone in the CNR is expected to offer facilities that are much superior even to those available in HFIR, although again gamma heating will be a constraint.

In HFIR, a group of facilities in the removable beryllium reflector around the control plates is also used for materials irradiation testing. The present modification program will raise the number of these facilities from 4 to 8 (all instrumented) and their diameter from 37 to 48 mm. Comparable facilities in the CNR will lie just outside the reactor core.

For CNR experiments requiring a lower fast-to-thermal flux ratio (such as fuel performance experiments), many positions are available further out in the reflector (~1.5 m from core centerline).

2.4 Analytical Applications

Various studies including neutron activation and neutron radiography will be possible with the CNRR. A detailed report on analytical techniques is being prepared by the National Bureau of Standards, and a summary of it will be presented when available.

2.5 Nuclear Physics

The nuclear physics applications can be divided into three parts: (1) properties of the neutron, (2) fundamental interactions, and (3) standard nuclear physics.

The neutron properties to be measured are electric charge, electric dipole moment, magnetic dipole moment, neutron mass, neutron half-life, and neutron decay parameters. Fluxes available from the CNRR should be more than adequate to accomplish experiments in these areas.

The topic of fundamental interactions includes strong interactions (studied in neutron-neutron collisions) and weak interactions (neutron-proton capture). A need for intense polarized neutron fluxes of 10^{20} neutrons$\cdot m^{-2} \cdot s^{-1}$ has been identified, but the energy distribution of this beam has not been defined.

Standard nuclear physics includes beta and gamma spectrometry, parity violation experiments, and neutron spin experiments. While the fluxes needed for these experiments have not been specified, the need for a large number of stations has been identified. Several of these will utilize cold or ultra-cold neutrons.

3. REACTOR PHYSICS

F. C. Difilippo R. T. Primm III

3.1 Introduction

Studies have focused on refinement of the reactor core geometry. Specifically, significant effort has been spent on examining various fuel distributions to determine which design offers the minimum peak-to-average power distribution over the lifetime of the core. Some effort was spent benchmarking the codes and cross-section libraries against the HFIR and the ILL reactor.

3.2 Analytical Calculations That Define Reactor Materials

A review of fundamental reactor physics principles can aid in translating the project criterion of producing a thermal flux in the reflector of 5 to 10 × 10^{19} neutrons•m^{-2}•s^{-1} into a realistic reactor design.

The optimization of the design is related to the problem of slowing down and diffusion of neutrons from a spherical fission source immersed in a moderator. This problem can be solved analytically allowing very inexpensive scoping calculations of the more important parameters. The first step toward the solution is the calculation of the Green's functions:

$$\nabla^2 G_i - \frac{G_i}{L_i} + \frac{1}{D_i} \delta(r - r') = 0 \ , \tag{3.1}$$

where G_i (r, r′) are the two-region diffusion kernels corresponding to a shell source located at r′; index i is equal to 1 for the core and equal to 2 for the reflector; and L_i and D_i are, respectively, the diffusion length and the diffusion constant of region i. The thermal fluxes are given by

$$\phi_i (r) = \int_0^\infty 4\pi r'^2 G_i(r,r')S(r')dr' \ , \tag{3.2}$$

where $S(r')$ is the slowing-down density evaluated at thermal energies. Fermi age theory can be used to evaluate S in terms of the ages of region i, τ_i, assuming a flat fission rate. In this way it is possible to find an explicit analytical form for the flux in terms of exponential and error functions. Table 6 (cases 2 to 5) shows an application of the model to the case of spherical cores moderated and reflected with D_2O using aluminum-clad U-235 fuel elements. The parameters not appearing in Table 6 are L_2 = 184 cm, D_2 = 0.831 cm, τ_2 = 131 cm^2 (pure D_2O), and τ_1 = 357 cm^2 (Al + D_2O mixture). Table 6 also shows results corresponding to the ideal case of a point source of fission neutrons, and in all cases the sources were scaled according to the energy release per fission. The required powers to produce a specified flux predicted by the analytical model were compared with the predictions of a numerical model, and excellent agreement (discrepancies around 1%) was found. The flux-to-power ratio is then determined by the eight parameters L_1, D_1, τ_1, L_2, D_2, τ_2, V, and d. Table 6 (column F) shows that the combined effect of large power density (i.e., small core volumes) and large neutron ages

Table 6. Power (P) to produce a 10^{20} neutrons$\cdot m^{-2}\cdot s^{-1}$ thermal flux[a]

Case	V (L)[b]	L_1 (cm)	D_1 (cm)	P (MW)	ρ (MW/L)[c]	F[d]
1	0.0			50.0	∞	1.000
2	40.0	3.15	0.849	193.0	4.82	0.906
3	60.0	5.11	1.026	214.0	3.57	0.872
4	90.0	6.48	1.091	251.0	2.79	0.830
5	120.0	7.46	1.123	285.0	2.37	0.795

[a]Spherical designs, D_2O moderator/reflector (thickness d = 100 cm), 42% metal fraction, only critical loading (zero core life).

[b]Volume of the core.

[c]Power density.

[d]Fraction of fission neutrons moderated in the reflector.

(i.e., poor moderators) results in a large fraction of the fission neutrons being moderated in the reflector; these neutrons are trapped there if a thick and low-absorbing reflector is used. The idealized case of a point source gives the minimum power required to create a neutron field with a fission source.

The use of a low-absorbing reflector (e.g., D_2O or Be) fixes τ_2 and L_2, leaving V_1, τ_1, and L_1 as the only free parameters in the design. The efficiency increases monotonically by reducing V_1 and by increasing τ_1 and L_1. High efficiencies are then obtained by reducing the core volume (i.e., increasing the power density ρ), by increasing the escape of fast neutrons from the core to the reflector (i.e., using a less efficient moderator like D_2O), and by reducing the core life (i.e., reducing the fuel loading). This behavior is illustrated in Fig. 7, where the P,ρ relationship that produces a peak thermal-neutron flux of 10^{20} neutrons$\cdot m^{-2}\cdot s^{-1}$ in the reflector is shown for critical loading and for critical loading plus 4.5 kg U-235 (with the necessary amount of ^{10}B to keep the system critical). The numerical model uses the VENTURE code

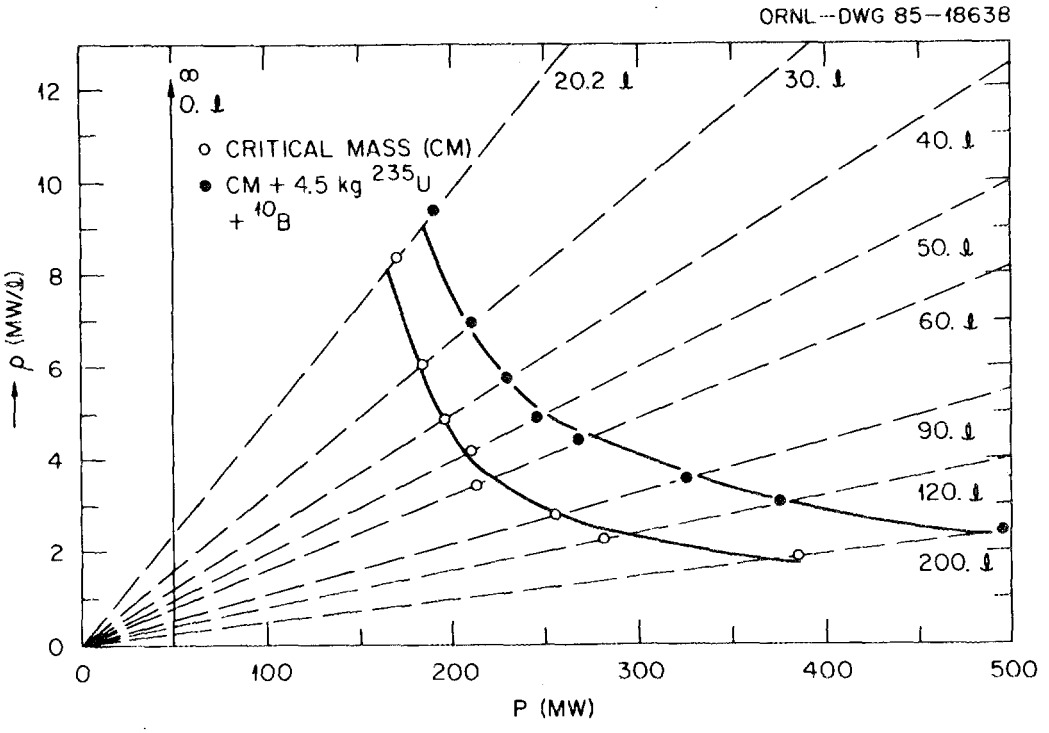

Fig. 7. Combinations of power and power density which yield a peak thermal flux in the reflector of 10^{20} neutrons$\cdot m^{-2}\cdot s^{-1}$.

(Sect. 3.4) and an appropriate six-energy-group cross-section set (Sect. 3.3). The vertical asymptotic line in Fig. 7 corresponds to the scaling (50 MW) of a point source of fission neutrons obtained with the analytical model.

The continuous lines in Fig. 7 correspond to the correlation

$$\phi = \frac{\alpha P^{1/3} \rho^{2/3}}{\left(1 + \frac{\delta}{R_c}\right)^2} , \tag{3.3}$$

where R_c is the radius of the core and δ,α are fitting constants for each type of loading. Equation (3.3) has a pole in the ρ,P plane at $P = \phi(4\pi/3)^{2/3}\ \delta/\alpha$. The correlation enables one to relate the numerical model to the analytical model. Figure 7 shows that about 200 MW can be saved if the average power density can be increased from 2 MW/L (present HFIR) to 8 MW/L; the pole at 50 MW reduces the sensitivity of P with respect to ρ for core volumes smaller than 30 L.

3.3 Cross-Section Sets

Two different cross-section sets were utilized in the calculations. A 123-group GAM-THERMOS library[9] was the source of cross-section data for one set of calculations. A 27-group library[9] derived from the Evaluated Nuclear Data File B — Version V (ENDF/B-V)[10] was the source of cross-section data for the second set of calculations.

For the GAM-THERMOS library, a spherical reactor model was used with the code XSDRNPM to collapse the 123-group cross-section set to three libraries containing 2, 4, and 6 energy groups, respectively. The spherical model is shown in Fig. 8. For the fuel zones, homogenized atom densities were input to the code, the homogenization based on the assumption of a 1.27-mm D_2O gap between fuel plates and a fuel clad thickness of 0.254 mm. The fuel "meat" was assumed to be 35 vol % U_3Si_2 and 65 vol % Al. The uranium was assumed to be 93% enriched in U-235.

For the ENDF/B-V calculations, a slab model was used with the XSDRNPM code to collapse the 27-group library to four groups. The cross

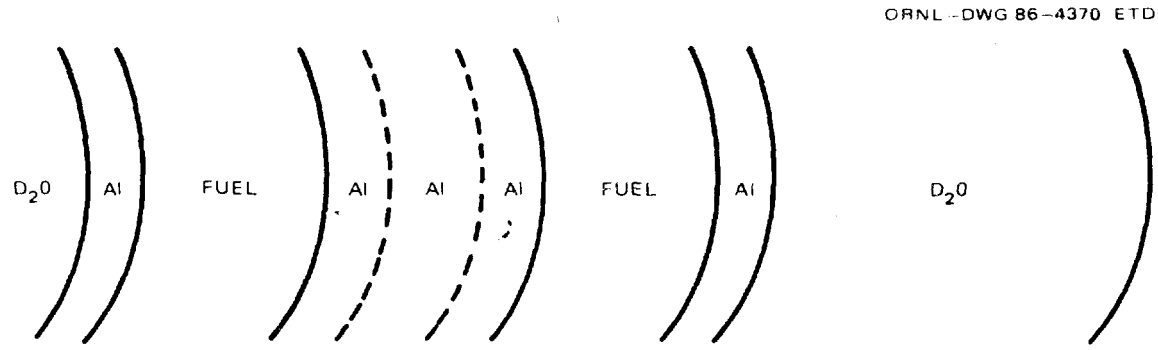

Fig. 8. One-dimensional spherical model used to collapse 123-group library.

sections were first spatially weighted using the model shown in Fig. 9. This weighting is necessary because the fuel thickness will vary as a function of radius as one moves outward from the center of the fuel element. A constant "meat" thickness was maintained by filling the remainder of the fuel plate with aluminum filter. After spatially weighting the 27-group cross sections, they were spectrally weighted using a cylindrical model similar to that shown in Fig. 8. The number of energy groups was reduced from 27 to 4 with energy boundaries of 10^{-5} eV, 0.4 eV, 100 eV, 100 keV, and 20 MeV.

3.4 Neutronics Codes

The VENTURE code system was utilized[11] to calculate fluxes, reactivity, and core lifetime. The system is based on diffusion theory and includes modules that allow for depletion and control rod movement calculations.

3.5 Benchmarking of Codes and Libraries

The VENTURE system was verified for both cross-section libraries for the HFIR and the ILL reactor. The results of these calculations are presented in Table 7. The G/T abbreviation represents six-group cross sections derived from the GAM-THERMOS library. The ENDF/B-V designation represents four-group cross sections derived from the point data in the Evaluated Nuclear Data File.

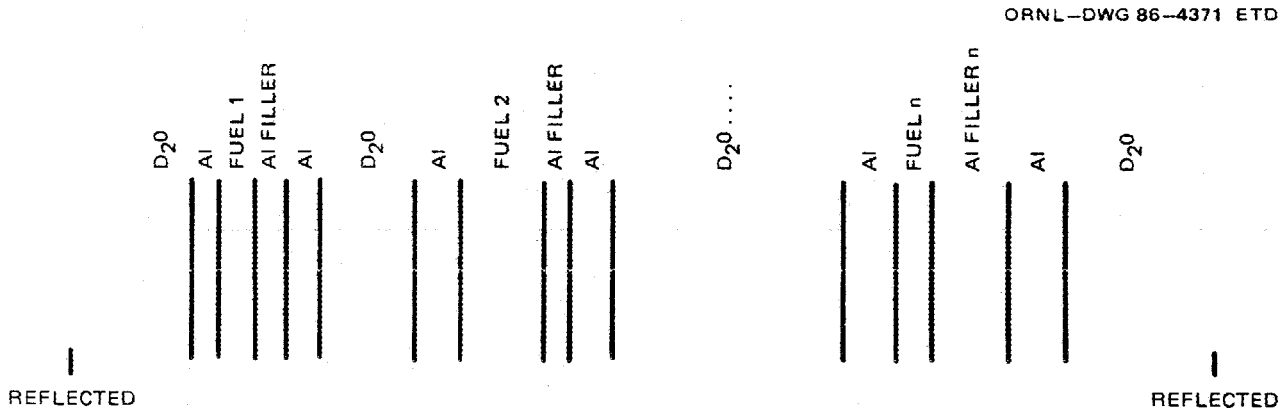

Fig. 9. One-dimensional slab model used to collapse 27-group library.

Table 7. Benchmarking of ILL and HFIR cores with the VENTURE system

Neutron energy range	Peak flux 10^{19} neutrons•m^{-2}•s^{-1}		
	Reported	G/T	ENDF/B-V
Thermal (EOL[a])			
ILL	1.5	1.5	1.5
HFIR	5.5	3.3	4.6
Epithermal (BOL[b])			
ILL		0.7	1.77
HFIR		0.76	1.42
Fast (BOL)			
ILL		0.65	0.92
HFIR	4.0[c]	1.5	2.0
Reactor core lifetime, d			
ILL	44	47	>49
HFIR	23	25	32

[a]EOL — end of life.

[b]BOL — beginning of life.

[c]Sum of epithermal and fast.

Some important differences exist between calculations performed with each of the two libraries, the major one being the cycle length with ENDF/B-V cross sections. The discrepancy is believed to be due to the lack of lumped fission product data in the ENDF/B-V library. In the G/T library, two "dummy" nuclides are present that represent slowly saturating and nonsaturating fission products. Corresponding data are not found in the ENDF/B-V library. However, future plans include generation of these nuclides.

3.6 Reference Core Design

A pair of cylinders containing involute-shaped fuel plates was chosen for the core design. The geometry of the core is nearly the same as that for HFIR (see Fig. 1).

Two possible annular configurations are shown in Fig. 10. The concentric ring design offers the advantage of easily varying the fuel concentration in the radial direction. However, the involute plate design offers the advantages of simpler fabrication — (1) only one type of plate is required (per element), (2) reduced cost for rejecting improperly prepared plates (because each plate is small), and (3) the lack of plate spacers (which can be a source of erosion and high local fuel temperatures).

As mentioned previously, the fuel was assumed to be uranium silicide clad with 0.25-mm-thick aluminum cladding. Materials other than aluminum

ORNL-DWG 86-4372 ETD

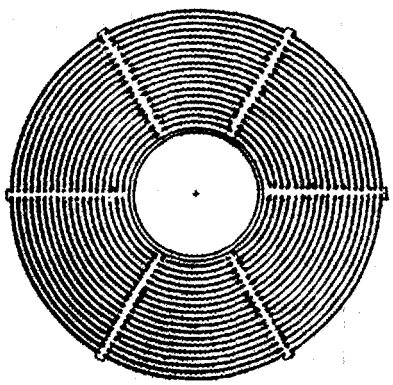

(a) CONCENTRIC RING DESIGN

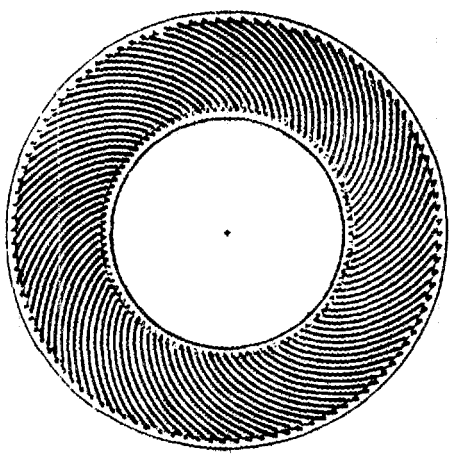

(b) INVOLUTE PLATE DESIGN

Fig. 10. Possible fuel plate configurations in annular geometry.

were examined neutronically. Zircaloy was found to have low neutron absorption but poor thermal conductivity relative to aluminum, meaning that a cladding thick enough to support a fuel plate would yield a fuel centerline temperature that would be too high. Stainless steel was evaluated, but the relatively high absorption cross section resulted in a reactivity loss that was judged to be too large ($\Delta k/k \approx 0.04$).

The dimensions of the core are provided in Fig. 1. The active fuel height of 350 mm was derived from thermal-hydraulic considerations. The additional 50 mm on each end of the fuel element is needed to achieve proper flow patterns within the element.

The radial dimensions of the core were influenced by the HFIR design yet were also derived from an optimization study. The following argument forms a basis for selecting the inner and outer radii.

It is expected that the power level of the CNRR will be determined by economics and by the anticipated siting difficulties of constructing a very high power reactor. The federal regulations in 10 *CFR* 50 are applicable to research reactors with power levels <250 MW, which might therefore be considered as a possible maximum. The power density will be determined from materials considerations. For a given power and power density, the core volume is fixed. However, an infinite number of combinations of radius and height correspond to a fixed volume. The optimum height and diameter can be determined by using steady-state diffusion theory and the equation for the area of a cylinder.

The one-group diffusion equation in cylindrical coordinates is

$$\frac{1}{r}\frac{\partial}{\partial r}\frac{r\,\partial\phi}{\partial r} + \frac{\partial^2\phi}{\partial^2 z} + B^2\,\phi = 0 \ . \tag{3.4}$$

Solving this equation by separation of variables, the solution can be shown to be

$$\phi = C\,J_o\left(\frac{2.405r}{R}\right)\cos\left(\frac{\pi z}{H}\right) \ . \tag{3.5}$$

The coefficient B^2, termed the buckling, can be shown to be the following:

$$B^2 = \left(\frac{2.405}{R}\right)^2 + \left(\frac{\pi}{H}\right)^2 , \tag{3.6}$$

where R is the radius of the cylinder and H is the height.

While the CNRR core will be a D_2O reflected annulus, in the following derivation it will be represented by a bare cylinder. The surface area of a cylinder is given by the following expression

$$S = 2\pi R\ (R + H) . \tag{3.7}$$

Solving Eq. (3.6) for R^2 and substituting the expression into Eq. (3.7), Eq. (3.8) is obtained

$$S = \frac{2\pi(2.405)^2}{B^2 - \pi^2/H^2} + \frac{2\pi H(2.405)}{\sqrt{B^2 - \pi^2/H^2}} . \tag{3.8}$$

For a given power level, the reactor with the minimum surface area will yield the maximum flux in the reflector. Differentiating Eq. (3.8) with respect to H and setting the result equal to zero, Eq. (3.9) is obtained

$$0 = 47.47(H) + 9.87\ (H^2B^2 - \pi^2)^{1/2} - H(H^2B^2 - \pi^2)^{3/2} . \tag{3.9}$$

This equation can be solved numerically by fixing either B^2 or H and searching for the solution of the resulting single-variable equation. Note that if B^2 is fixed, a fourth-order polynomial in H is generated. One would expect to find a pair of positive roots for each value of B^2 (the negative roots are physically unrealistic).

The corresponding value of the radii are found by substituting the (H,B^2) solution into Eq. (3.6). This procedure yielded the results shown in Table 8 (smaller radius of pair is shown). The CNRR height and outer radius are almost exactly the same as the optimal dimensions for a bare cylinder.

The inner radius of the CNRR was selected to be essentially the same as the HFIR. Two criteria were important in the selection of the inner radius: involute plate length and criticality safety. Studies performed

Table 8. Optimal dimensions for a bare cylindrical reactor

Height (cm)	Radius (cm)	Buckling (cm^{-2})
10	6.31	0.2442
15	9.46	0.1085
20	12.61	0.0611
25	16.04	0.0383
30	18.92	0.0271
35	22.45	0.0195
40	23.63	0.0165
45	28.37	0.0121
50	29.54	0.0105
55	30.62	0.0094
60	37.83	0.0068
65	39.01	0.0061
70	40.12	0.0056

as a part of the HFIR program showed that involute plates with a plate length longer than 8 cm were insufficiently rigid.[12] Additionally, the reactor core must remain subcritical during the fabrication and transportation-to-reactor procedures. The easiest method of maintaining subcriticality is to divide the core into two rings, each of which will be subcritical. These considerations, along with the thickness of the desired interfuel zone and fuel element side plates, led to the selection of an inner radius of 64 mm for the inner side plate of the inner element.

As noted previously, the clad thickness of the CNRR fuel plates is 0.254 mm. The thickness of the fuel region inside a plate varies (Al-filler material is also present in the plate) but is never more than 0.762 mm (30 mil). The fuel plate spacing was assumed to be 1.27 mm (50 mil).

3.6.1 Graded fuel distribution

The CNRR is an undermoderated reactor. Neutrons born in the core will usually escape to the reflector where they are moderated and may drift back to the reactor core. Thus, fuel at the outermost radial and

axial positions in the fuel plates will "see" a large thermal flux. Consequently, if fuel were equally distributed throughout the plate, local power densities at the radial and axial edges of the plates would be much greater than the average power density. These edge peaks can be more than twice the average power density and, if uncorrected, will severely limit the maximum reactor power.

One method of smoothing the power distribution is to place less fuel at the edges of the plates than at the center. This "grading" of the fuel distribution is currently performed in the radial direction for the HFIR fuel plates. Examination of the flux distribution for an early CNRR design revealed that some correction for flux peaking was needed in both the radial and axial directions. (HFIR does not have a beryllium reflector in the axial direction, which leads to a lower axial peak than the CNRR core that is completely surrounded by reflector.) Rather than lose neutrons to a burnable poison or control rod, it was decided to grade the fuel axially and radially. The goal of the grading was to maintain as flat a power distribution as possible over the entire fuel cycle. Because the location of the hot spot varied with time, finding a fuel distribution that maintained a minimum peak-to-average power distribution over the whole cycle was an iterative process.

Three procedures were examined: minimizing the peak-to-average power ratio at beginning-of-cycle, at middle-of-cycle, and at end-of-cycle. Intuitively, one would expect that minimizing peak-to-average power would be less advantageous at beginning-of-cycle than at other times because initially little or no oxide coating would be present on the clad; thus, for a given power density, fuel centerline temperatures would be lower than later in the cycle. Therefore, a somewhat higher peak-to-average power ratio could be tolerated at beginning-of-cycle than later in the cycle.

The grading was obtained by iteration of the equation

$$C_{j+1} = C_j \frac{\bar{\rho}}{\rho_j(\mathrm{BOL})} x_j \ , \qquad (3.10)$$

where C is the fuel concentration at a given point, j is the iteration

number, $\overline{\rho}$ is the average power density, and ρ(BOL) is the power density at beginning of life (BOL) at the same point. Parameter x_j is an adjustable factor between 1 (to optimize the power distribution at BOL) and

$$x_j(\mathrm{EOL}) = \frac{\rho_j(\mathrm{BOL})}{\rho_j(\mathrm{EOL})} + \mathrm{at}\ \overline{\rho}_j \frac{\rho_j(\mathrm{BOL})}{\overline{\rho}C_j}\left[1 - \frac{\overline{\rho}}{\rho_j(\mathrm{EOL})}\right] \tag{3.11}$$

[to optimize the power distribution at EOL (end of life)]. In Eq. (3.11), t (in days) is the core life, $\overline{\rho}_j = 0.5\ [\rho_j(\mathrm{BOL}) + \rho_j(\mathrm{EOL})]$, and a = 3.178×10^6/b•cm•MW.

The fuel grading that optimizes the power distribution at medium core life (half way through the fuel cycle) is shown in Table 9. Only the upper half of the core is described because the fuel distribution was assumed to be symmetric about the core axial centerline. For the fueled region of both the inner annulus (radii of 71.3 to 126.3 mm) and outer annulus (radii of 165.3 cm to 219.7 mm), a radial mesh of eight equal intervals in each element was assumed. Axially, the core was divided into five zones. A plot of the fuel grading is shown in Fig. 11.

The data in Table 9 were used to develop various correlations. Equation (3.12) is a least-squares fit to the data and can be used to generate atom densities for U-235 in units of atoms per barn•centimeter for the inner element.

$$[\mathrm{U\text{-}235}] = -1.12(10^{-4})\ r^2 + 2.30(10^{-3}) \times r - 8.59(10^{-6})\ z^2 - 0.00882\ . \tag{3.12}$$

Both the radius r and the height z are in centimeters. The zero point for the radius is the center of the annulus, and the zero point for the height is at the axial midpoint of the annulus. The value of R^2, a measure of the goodness of the fit of the correlation to the data, is 0.92. This means that the fitted regression equation explains 92% of the variation among atom densities.

Table 9. Fuel distribution for reference core

Node	Nodal coordinates[a]		^{235}U (1/b•cm)	^{238}U (1/b•cm)	g U/cm^3 ("meat")
	r	z			
1	7.47	1.75	0.001745521	0.000131438	2.4433
2	7.47	5.25	0.001588406	0.000119607	2.2234
3	4.47	8.75	0.001287212	0.000096927	1.8018
4	7.47	12.25	0.000909875	0.000068514	1.2736
5	7.47	15.75	0.000600171	0.000045193	0.8401
6	8.16	1.75	0.002436136	0.000183441	3.4100
7	8.16	5.25	0.002201463	0.000165770	3.0815
8	8.16	8.75	0.001706950	0.000128533	2.3893
9	8.16	12.25	0.001073877	0.000080863	1.5031
10	8.16	15.75	0.000631460	0.000047549	0.8839
11	8.85	1.75	0.002786211	0.000209802	3.9000
12	8.85	5.25	0.002786211	0.000209802	3.9000
13	8.85	8.75	0.002228594	0.000167813	3.1194
14	8.85	12.25	0.001242395	0.000093552	1.7390
15	8.85	15.75	0.000653978	0.000049244	0.9154
16	9.54	1.75	0.002786211	0.000209802	3.9000
17	9.54	5.25	0.002786211	0.000209802	3.9000
18	9.54	8.75	0.002772366	0.000208759	3.8806
19	9.54	12.25	0.001374957	0.000103534	1.9246
20	9.54	15.75	0.000670876	0.000050517	0.9391
21	10.22	1.75	0.002786211	0.000209802	3.9000
22	10.22	5.25	0.002786211	0.000209802	3.9000
23	10.22	8.75	0.002786211	0.000209802	3.9000
24	10.22	12.25	0.001416377	0.000106653	1.9826
25	10.22	15.75	0.000678714	0.000051107	0.9500
26	10.91	1.75	0.002786211	0.000209802	3.9000
27	10.91	5.25	0.002786211	0.000209802	3.9000
28	10.91	8.75	0.002723547	0.000205083	3.8123
29	10.91	12.25	0.001310312	0.000098666	1.8341
30	10.91	15.75	0.000675005	0.000050828	0.9448
31	11.60	1.75	0.002786211	0.000209802	3.9000
32	11.60	5.25	0.002786211	0.000209802	3.9000
33	11.60	8.75	0.002120493	0.000159673	2.9681
34	11.60	12.25	0.001156619	0.000087093	1.6190
35	11.60	15.75	0.000662298	0.000049871	0.9270
36	12.29	1.75	0.002786211	0.000209802	3.9000
37	12.29	5.25	0.002436825	0.000183493	3.4109
38	12.29	8.75	0.001595107	0.000120112	2.2327
39	12.29	12.25	0.000987272	0.000074342	1.3819
40	12.29	15.75	0.000639270	0.000048137	0.8948
41	16.87	1.75	0.002786211	0.000209802	3.9000
42	16.87	5.25	0.002338098	0.000176059	3.2727
43	16.87	8.75	0.001505847	0.000113390	2.1078
44	16.87	12.25	0.000935763	0.000070463	1.3098
45	16.87	15.75	0.000610653	0.000045982	0.8548

Table 9 (continued)

Node	Nodal coordinates[a]		^{235}U (1/b•cm)	^{238}U (1/b•cm)	g U/cm^3 ("meat")
	r	z			
46	17.55	1.75	0.002786211	0.000209802	3.9000
47	17.55	5.25	0.002475696	0.000186420	3.4653
48	17.55	8.75	0.001612286	0.000121405	2.2568
49	17.55	12.25	0.000970249	0.000073060	1.3581
50	17.55	15.75	0.000595232	0.000044821	0.8332
51	18.23	1.75	0.002253963	0.000169723	3.1550
52	18.23	5.25	0.001947062	0.000146614	2.7254
53	18.23	8.75	0.001420556	0.000106968	1.9884
54	18.23	12.25	0.000919672	0.000069251	1.2873
55	18.23	15.75	0.000572194	0.000043086	0.8009
56	18.91	1.75	0.001608566	0.000121125	2.2516
57	18.91	5.25	0.001463172	0.000110177	2.0481
58	18.91	8.75	0.001174615	0.000088448	1.6442
59	18.91	12.25	0.000836824	0.000063013	1.1713
60	18.91	15.75	0.000546393	0.000041143	0.7648
61	19.59	1.75	0.001186816	0.000089367	1.6612
62	19.59	5.25	0.001113605	0.000083854	1.5588
63	19.59	8.75	0.000959704	0.000072266	1.3433
64	19.59	12.25	0.000745378	0.000056127	1.0433
65	19.59	15.75	0.000519273	0.000039101	0.7268
66	20.27	1.75	0.000921835	0.000069414	1.2903
67	20.27	5.25	0.000881349	0.000066366	1.2337
68	20.27	8.75	0.000795901	0.000059931	1.1141
69	20.27	12.25	0.000660786	0.000049757	0.9249
70	20.27	15.75	0.000489794	0.000036881	0.6856
71	20.95	1.75	0.000748760	0.000056382	1.0481
72	20.95	5.25	0.000724209	0.000054533	1.0137
73	20.95	8.75	0.000673048	0.000050681	0.9421
74	20.95	12.25	0.000586506	0.000044164	0.8210
75	20.95	15.75	0.000451316	0.000033984	0.6317
76	21.63	1.75	0.000628412	0.000047319	0.8796
77	21.63	5.25	0.000613086	0.000046165	0.8582
78	21.63	8.75	0.000579113	0.000043607	0.8106
79	21.63	12.25	0.000518580	0.000039049	0.7259
80	21.63	15.75	0.000418312	0.000031499	0.5855

[a](0,0) is centerline of annuli at core midplane.

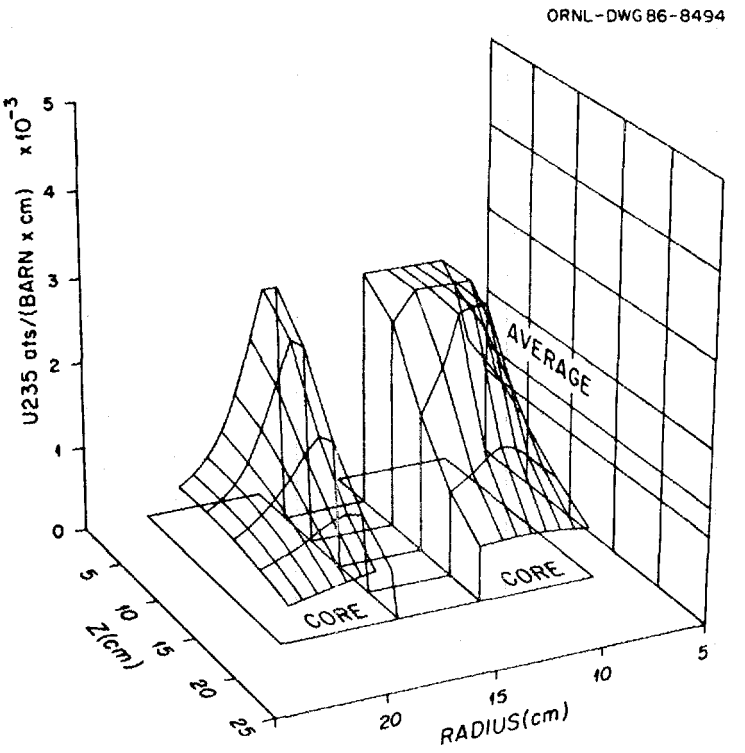

Fig. 11. U-235 concentration as a function of r and z for reference core.

Equation (3.13) can be used to generate atom densities for U-235 for the outer element.

$$[\text{U-235}] = -2.64(10^{-4})\ r - 8.16(10^{-5})\ z + 6.89(10^{-3})\ . \qquad (3.13)$$

The quantities [U-235], r, and z are the same as defined for Eq. (3.12). The value of R^2 for Eq. (3.13) is 0.77, that is, 77% of the variation among atom densities can be explained by this equation.

Note that a constraint on the fuel distribution iteration process is the upper limit for the uranium concentration. As the volumetric fraction of U_3Si_2 in the aluminum matrix is increased, the thermal conductivity of the fuel composite decreases. In the reference core, the maximum volumetric fraction of U_3Si_2 in the aluminum matrix is 35%. The average density of U_3Si_2 is 12.1 kg/L.* The corresponding uranium density in the fuel matrix would be 3.92 kg/L.

*Experiments managed by G. L. Copeland.

Involute plates are fabricated by first manufacturing a flat plate and then bending it to the proper shape. Fuel grading is accomplished by varying the thickness of the uranium-bearing region at various positions along the fuel plate. In regions where the fuel matrix thickness is less than the maximum possible value (0.762 mm), an aluminum filler is utilized. Hence, for fuel fabrication purposes, the fuel distribution should be reported as [fuel thickness = fn (x,z)] where x is the distance *along* the involute plate that corresponds to a given radius and z is the distance along the axial length of the plate. Equation (3.14) can be used to generate the fuel thickness at any point on an inner annulus fuel plate. (Note that z = 0 is at centerline of plate, x = 0 is at the inner edge.)

$$[\text{Fuel thickness}] = -1.44\ (10^{-3})\ x^2 + 1.20(10^{-2})\ |x| - 2.11\ (10^{-4})\ z^2 + 0.0491\ . \quad (3.14)$$

All variables are in centimeters. Equation (3.14) is derived from the data contained in Table 9, and thus the value of the correlation coefficient R^2 for Eq. (3.14) is the same as Eq. (3.12). Similarly, Eq. (3.15) can be used to calculate the fuel thickness at any point on an outer annulus fuel plate:

$$[\text{Fuel thickness}] = -5.52(10^{-3})\ x - 2.01(10^{-3})|z| = 0.0612\ . \quad (3.15)$$

Again, all variables are in centimeters, and, as expected, the correlation coefficient R^2 for this equation is 0.77, the same as found for Eq. (3.13).

The fuel inspection technique used with HFIR elements is an activation technique that senses activity per unit area. Thus, for the fuel grading equation to be of use to current inspection techniques, it must be in the form [areal density of uranium = f(x,z)] where again x is the distance along the involute plate that corresponds to a given radius r measured from the centerline of the annular element.

Equation (3.16), derived from data in Table 9, provides an expression for aerial density (units are g U/cm^2) as a function of x and z

(units are cm). Again the zero point for x is the inside edge of the plate and the zero point for z is at the axial centerline.

$$[\text{Areal density}] = -6.24(10^{-3})\ x^2 + 5.19(10^{-2})\ x - 9.16(10^{-4})\ z^2 + 0.212 \quad (3.16)$$

For the outer annulus fuel plates, Eq. (3.17) describes the areal fuel density distribution:

$$[\text{Areal density}] = -2.39(10^{-2})\ x - 8.69(10^{-3})|z| + 0.265\ . \quad (3.17)$$

3.6.2 Calculated flux distribution

Using the codes, cross sections, reactor dimensions, and the fuel distribution described in previous sections, the neutron flux and core lifetime were calculated. These calculations were performed with the four-group cross-section set derived from the 123-group library.

For the reference core with a power level of 246 MW, a cycle length of 14 d was calculated. Plots of the thermal, low epithermal, and fast flux for a power level of 246 MW as a function of position are given in Figs. 12–15. To obtain a peak thermal flux in the reflector of 10^{20} neutrons$\cdot m^{-2}\cdot s^{-1}$, the power level must be increased to 270 MW and the cycle length (without further addition of reactivity) would drop to 12.8 d. Flux ratios are provided in Figs. 16 and 17. Table 10 lists peak thermal flux in the reflector and peak localized power density in the core as a function of time. The value of the peak local power density is an important input to the thermal-hydraulic analyses. Even though the spatial mesh used in this problem was coarse, a significant amount of movement of the peak was observed.

It should be emphasized that the values shown in Figs. 12–15 and Table 10 are for a power level of only 246 MW. However, the flux values, power density, and cycle length scale directly with power level.

Note that the thermal flux increases during the fuel cycle. An increase in power of about 10%, to 270 MW, would produce an EOL peak thermal flux in the reflector of 10^{20} neutrons$\cdot m^{-2}\cdot s^{-1}$.

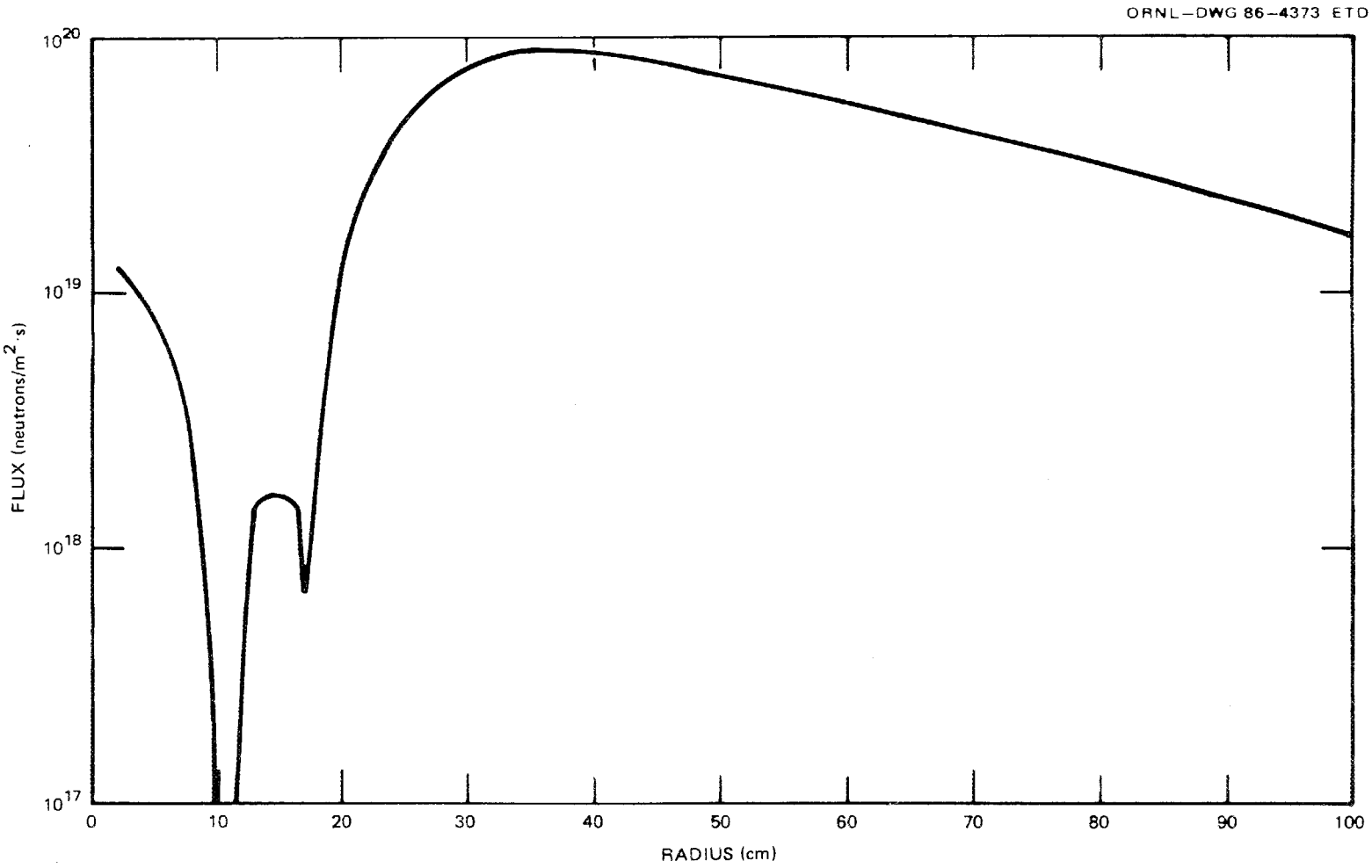

Fig. 12. Radial distribution of thermal flux in reference core.

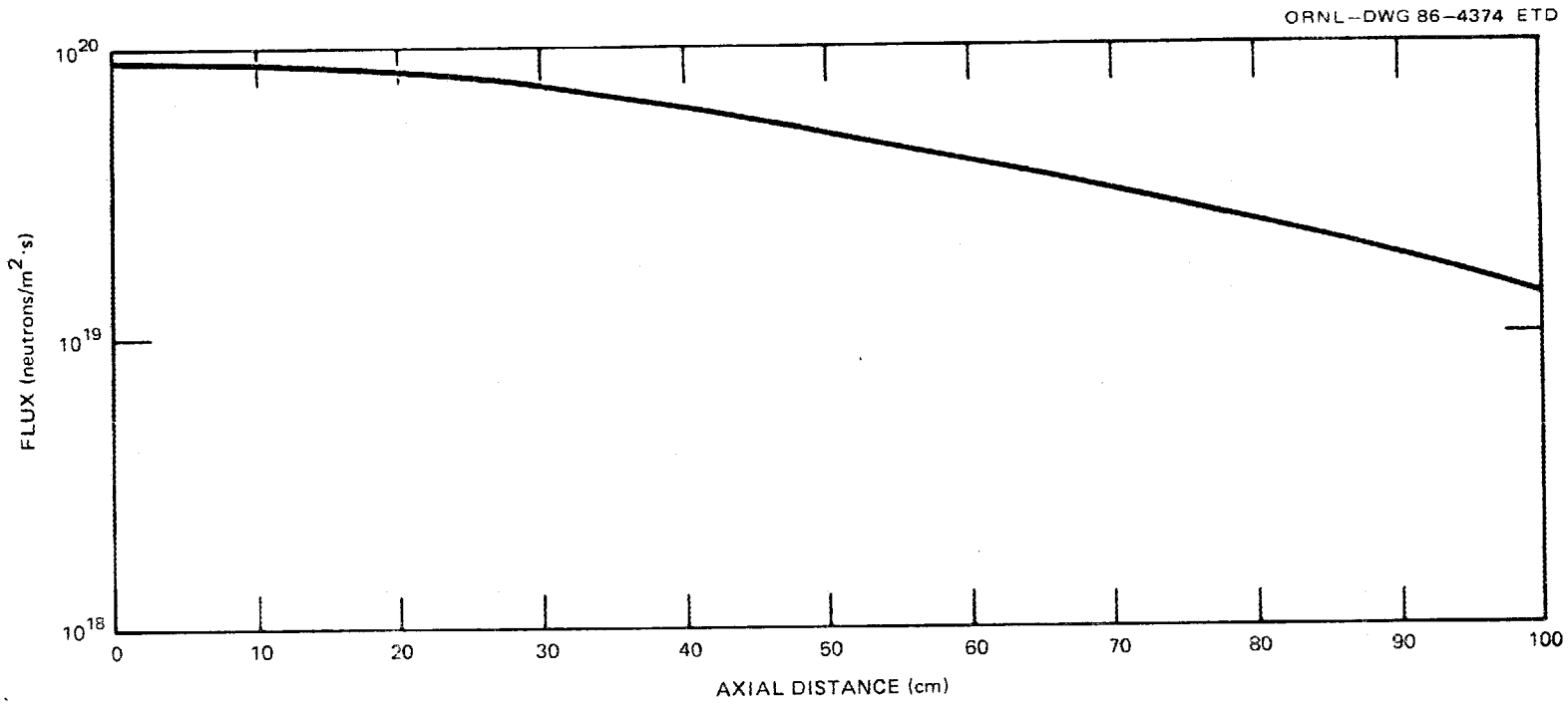

Fig. 13. Axial distribution of thermal flux in reference core.

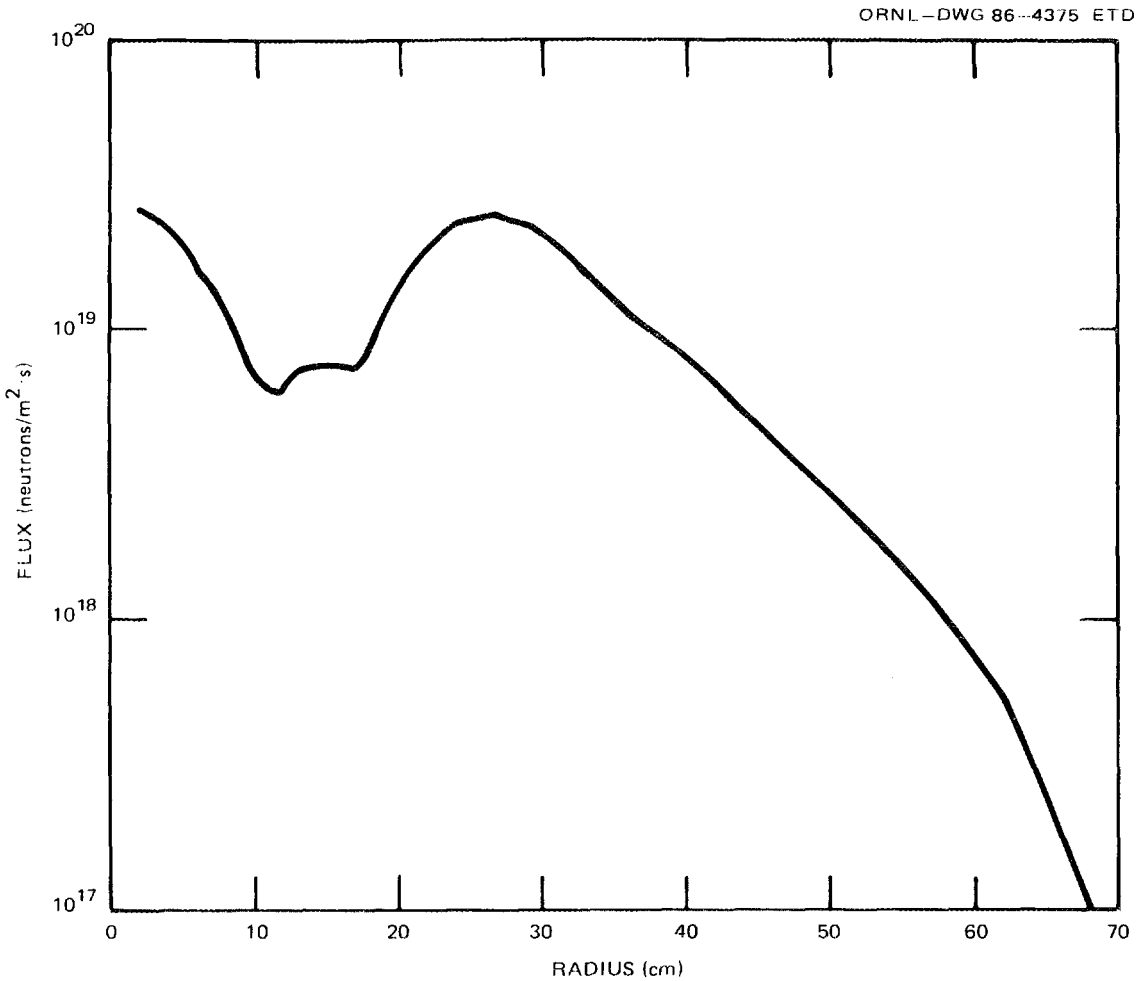

Fig. 14. Radial distribution of epithermal flux in reference core.

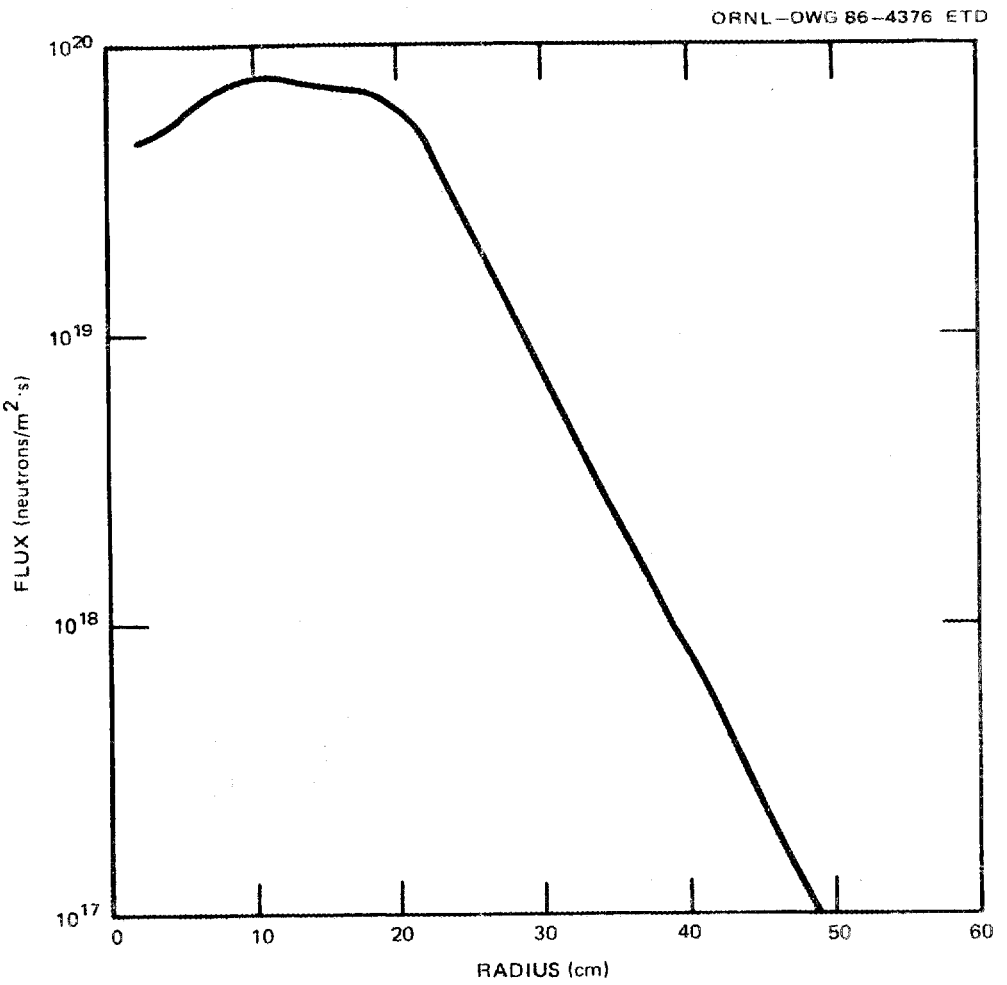

Fig. 15. Radial distribution of fast flux in reference core.

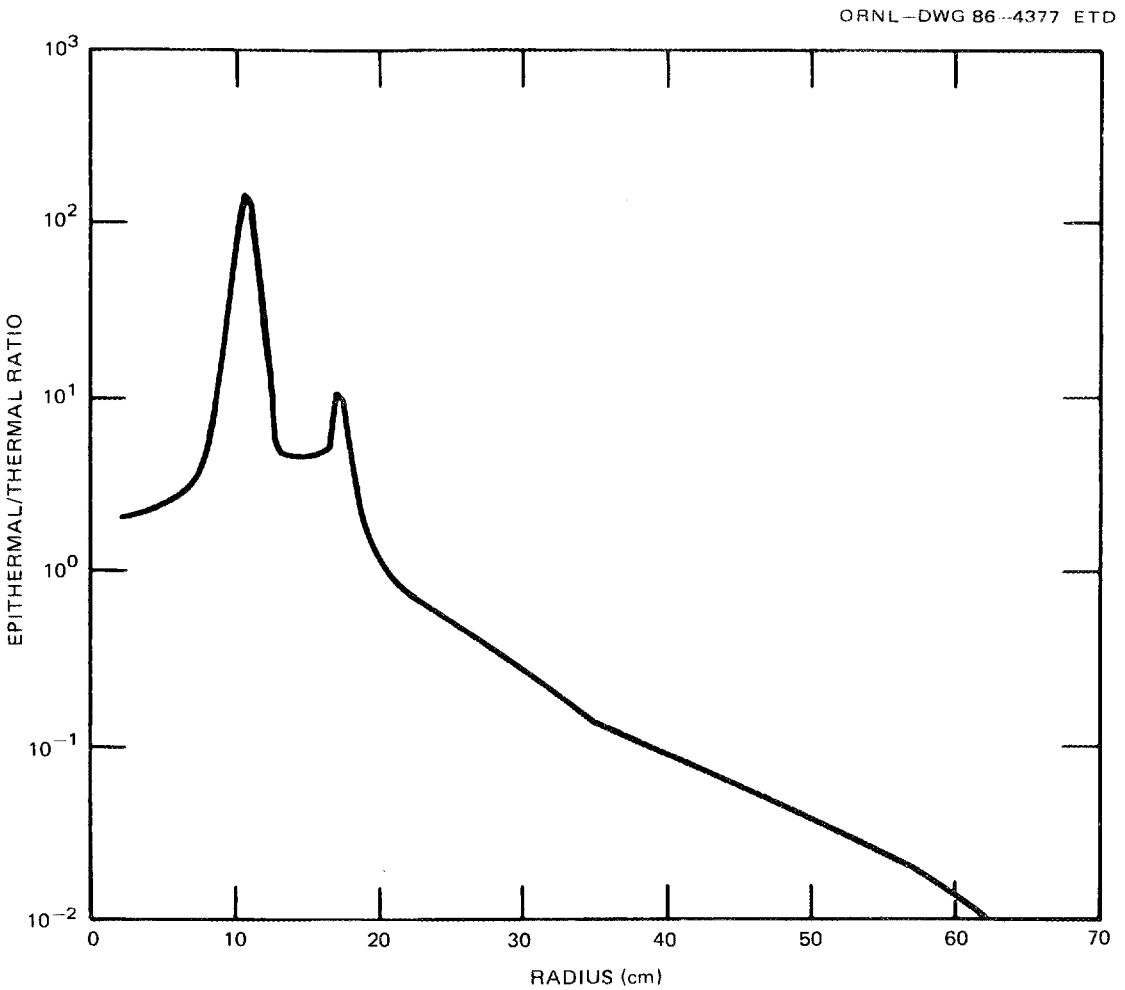

Fig. 16. Radial distribution of epithermal/thermal flux ratio (reference core).

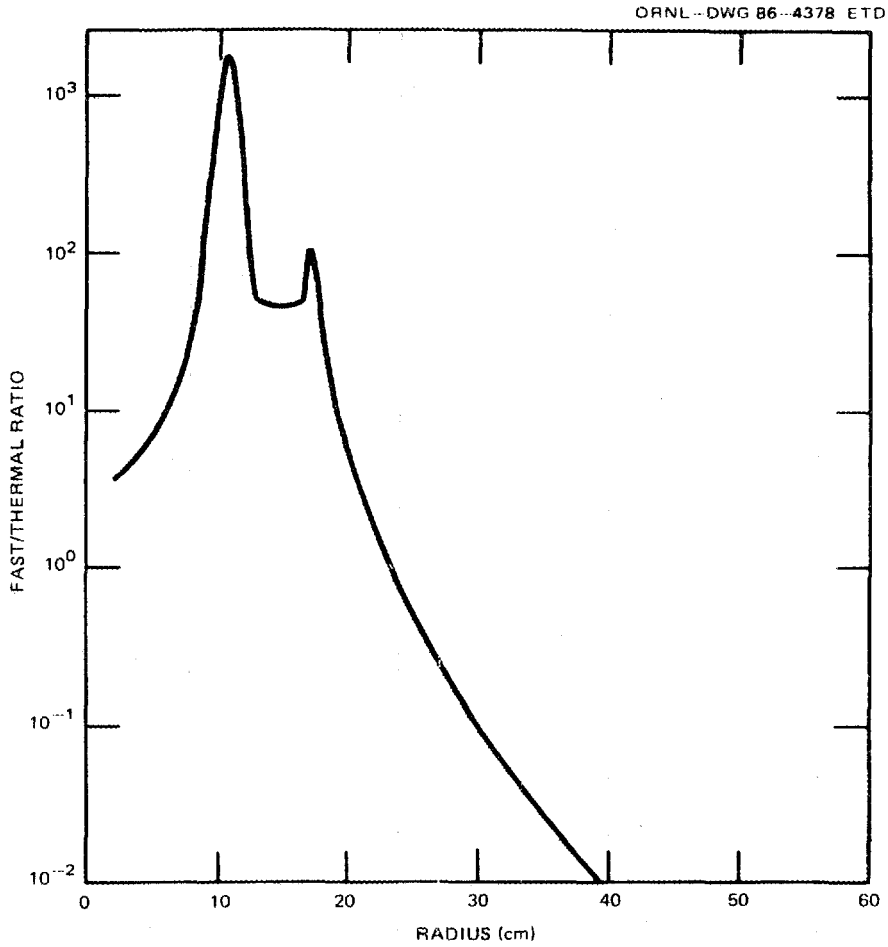

Fig. 17. Radial distribution of fast/thermal flux ratio (reference core).

Table 10. CNRR performance over a fuel cycle[a]

Time (d)	Peak thermal flux in reflector (10^{19} neutrons $m^{-2} \cdot s^{-1}$)	Maximum local power density (MW/L)	Location of maximum power density (node No.)[b]
0.0	7.04	11.22	80
3.5	7.69	9.89	76
7.0	8.07	8.89	69
10.5	8.48	9.32	54
14.0	8.98	10.25	53

[a]Power level in reactor core assumed to be 246 MW; average power density of 7.03 MW/L.

[b]See Table 9 for r,z coordinates.

4. THERMAL-HYDRAULIC DESIGN

W. R. Gambill

4.1 Introduction

Because the primary goal of this project is to attain a maximum steady-state value of thermal neutron flux much higher than that generated by any existing reactor, the maximum power density will also be quite large for reasonable values of reactor thermal power. This density, in turn, means high heat fluxes and, therefore, special attention to the details of the intensive cooling required as fuel plate limits are approached.

4.2 Coolant, Cladding, and Fuel Temperatures

Based on a generic (non-site-specific) heat rejection capability, the maximum design CNRR inlet D_2O temperature has been taken to be 49°C. To avoid expensive two-phase control (steam condensation) safety measures in the event of a loss-of-coolant accident, the maximum CNRR outlet bulk D_2O temperature has been limited to less than the normal boiling point of 101.4°C. Specifically, $(t_{b,o})_{max} = 99°C$.

To determine fuel plate surface temperatures, the local heat-transfer coefficient for nonboiling turbulent flow has been and will be calculated with the correlation of Petukhov[13] or of Hausen.[14] For CNRR conditions, the coefficients from these two correlations are in close agreement for Reynolds moduli $>10^4$, although the forms of the correlations are quite different. Because of its sound theoretical basis and excellent agreement with critically evaluated experimental data, the Petukhov relation now appears preferable.

The maximum fuel temperature is determined from the combination of variables giving the maximum value of

$$t_{fuel} = t_{b,l} + (\Delta t)_b + (\Delta t)_{film} + (\Delta t)_{oxide} + (\Delta t)_{clad} + (\Delta t)_{fuel\ core} .$$

For U_3Si_2, this value is believed to be ~354°C for the localized hot spot. In HFIR (U_3O_8 fuel), the calculated maximum is 327°C. At the same

volumetric loading, the thermal conductivity of U_3Si_2 is higher than that of U_3O_8, and the uranium content is significantly higher.

4.3 Fuel Plate Deflection, Vibration, and Erosion

These phenomena have caused no operational problems at the HFIR (V_{max} = 16.5 m/s) or at the Savannah River Plant (V_{max} = 22 m/s). Plate spacer elements are considered undesirable and are presently viewed as a last resort. Extensive experimental and analytical work in this area is planned. During the 1960s, tests at the Savannah River Laboratory (SRL) indicated that erosion of aluminum "would not be a problem in a well-designed fuel assembly until the velocities exceed about 30.5 m/s."[15] The general data base, based on short exposure times, is in agreement. Even an erosion rate of 1.27 mm/year would remove only about 0.05 mm of cladding in 15 d, the approximate core lifetime expected.

4.4 Critical Flow Velocity for Fuel Plates

A coolant $V > V_c$ corresponds to buckling collapse of one or more fuel plates. The general functional dependence is illustrated by that for the simplest case; that is, for a flat plate:[16]

$$V_c \propto \frac{(pt)^{3/2}\,(cg)^{1/2}}{(pw)^2} ,$$

for a given plate material and coolant, where pt = plate thickness, cg = coolant gap, and pw = plate width. This relation indicates, for example, that $(V_c)_{30} = 0.36\ (V_c)_{50}$, where $(V_c)_{30} = V_c$ for pt = cg = 0.76 mm, and $(V_c)_{50} = V_c$ for pt = cg = 1.27 mm. For plates, V_c decreases as the plate shape is changed from involute to uniformly curved to flat. A finite-element analysis for the V_c of involute plates has been developed, and for CNRR cores, this method has given $V_c \approx 92.8$ m/s at $t_{plate} = 204°C$ and $V_c \approx 78.5$ m/s at $t_{plate} = 316°C$. These values of V_c exceed the expected D_2O velocity by factors of 2.9 to 3.4.

4.5 Core Pressure Drop

Designs to date have generally produced a core $\Delta P < 1.8$ MPa. For the HFIR, the core $\Delta P = 0.69$ MPa. The primary system ΔP is expected to be about 1.6 $(\Delta P)_{core}$, as in the HFIR. For an anticipated mean surface roughness of 0.51 μm, the mean asperity height of the plate surface will be contained well within the laminar sublayer of the D_2O turbulent boundary layer ($\varepsilon/\delta_{bl} \approx 0.13$), and the surface will be hydrodynamically smooth. The smooth-surface, isothermal friction-factor correlations of Filonenko[17] and of Hermann[18] give very good agreement with measured HFIR core ΔP values, and the former has been and will be used for CNRR design.

4.6 The Incipient-Boiling Heat Flux (ϕ_{ib}) and the Critical Heat Flux (ϕ_c)

The incipient boiling heat flux ϕ_{ib} is presently the limit to the maximum local heat flux in the CNRR. The advantages of avoiding local boiling include a hot-spot void fraction $\rightarrow 0$, no local reactivity changes, and no two-phase flow instabilities. The correlations of Bergles and Rohsenow[19] and of Davis and Anderson[20] are in excellent agreement for both H_2O and D_2O. An unresolved question relates to the effect of dissolved tritium on the ϕ_{ib}. In the CNRR, detritiation is planned, which will minimize or eliminate any decrement in ϕ_{ib}.

Values of ϕ_c up to 46 MW/m^2 have been experimentally attained with aluminum heaters. As a design correlation, either the superposition method of Gambill[21] or a modification of a similar approach by Kutateladze and Leont'ev[22] will be used. A reasonable margin between ϕ_{ib} and ϕ_c is desirable (greater than ~25%). The flow-channel equivalent diameter should exceed a critical diameter that decreases with pressure, as shown in Fig. 18 for H_2O. A remaining question relates to how the ϕ_c of D_2O compares with that of H_2O at constant conditions. SRL data at $P = 0.20$ to 0.66 MPa indicate a consistent 16% increment for D_2O on either aluminum or stainless steel.[23] However, the hydrodynamic correlations of ϕ_c give, for the velocities, pressures, and subcoolings of interest, values of the ratio $(\phi_c)_{D_2O}$: $(\phi_c)_{H_2O}$ of 1.0 (±0.1).

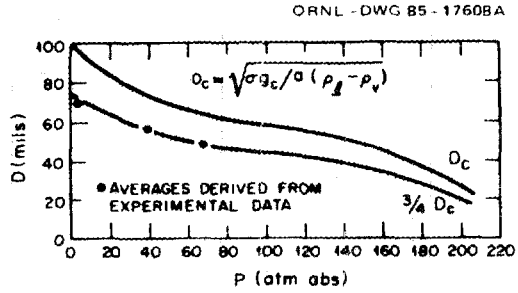

Fig. 18. Dependence of critical channel diameter on pressure for H_2O.

4.7 Coolant Pressure Level

The ϕ_{ib} increases with pressure; the ϕ_c also increases with pressure, but more slowly than ϕ_{ib}. The ratio ϕ_c/ϕ_{ib}, therefore, decreases with pressure, as illustrated by a curve calculated for the HFIR,[24] shown as Fig. 19. At high D_2O velocities, there is little increase in ϕ_c at pressures exceeding ~6.9 MPa. For these reasons, emphasis has been placed on P_o = 4.1 to 6.9 MPa, at which level adequate values of ϕ_{ib} are generated for V = 24.4 to 30.5 m/s.

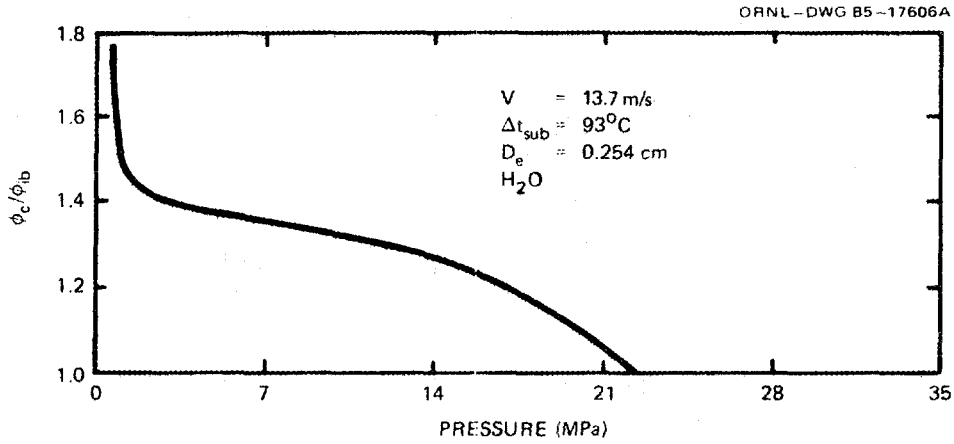

Fig. 19. Dependence of the ratio of critical to incipient-boiling heat fluxes on pressures.

4.8 Power Density Profile and Surface Area Density

A high power density is needed to achieve a high thermal-neutron flux per unit of reactor power. This leads to a small core volume that,

in turn, necessitates a high ratio of heat transfer surface area to volume. The ratio of maximum-to-average power densities should be minimized; our goal is a (hot-spot) maximum-to-average power density ratio of 2. For parallel-plate fuel elements, the heat flux is given by the expression

$$\phi = \frac{q'''}{2\ (MF/pt)} ,$$

where ϕ is in megawatts per square meter, q''' is in megawatts per liter, and pt is in millimeters. The heat flux for a given power density decreases as the ratio of metal fraction to plate thickness increases.

4.9 Maximum Core Power Density

The various factors considered may be combined to produce the parametric depiction in Fig. 20; for the range of cases considered, the maximum (hot spot) power density exceeds 11 MW/L when the peak heat flux equals the incipient-boiling value. The three-part parameter (MF/pt, $\Delta t_{sub,\ min,o}$, V) for the reference CNRR design is closely approximated by the curve labeled 3.9/150/21, for which the maximum power density is seen to approach 18 MW/L. These high levels of power density are permissible only if the oxide thickness on the cladding is virtually zero; otherwise, the plate centerline temperature is excessively high.

4.10 Core Thermal/Flow Analysis Code

The code previously developed for the HFIR[25] has been modified to incorporate the physical and thermodynamic properties of D_2O as well as those of H_2O. It will soon be further modified with the updated thermal and flow correlations mentioned previously.

4.11 Results for the Reference Core

The results for the subject core design are summarized in Tables 11–13. With oxide on unmodified cladding present to the extent expected,

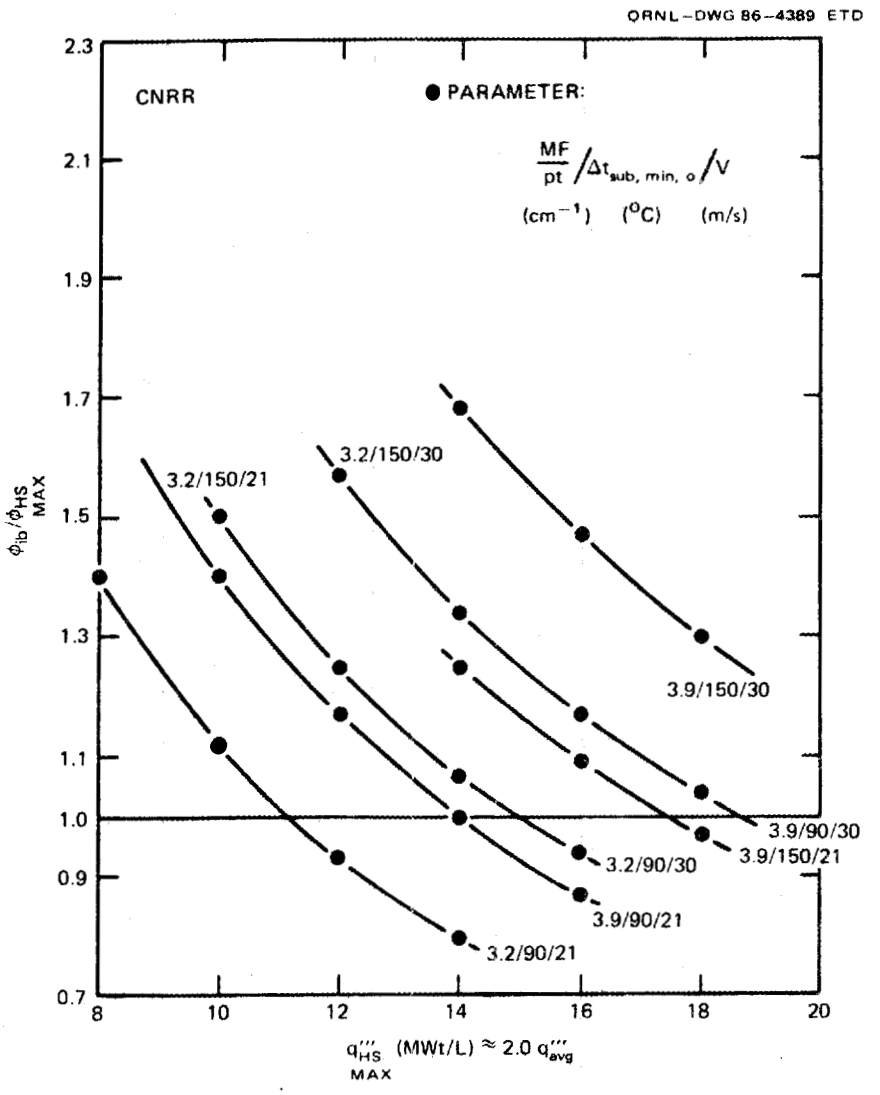

Fig. 20. Parametric incipient-boiling depiction for D_2O at P = 6.9 MPa.

the core could be operated at powers up to 135 MW, and the peak unperturbed thermal neutron flux in the reflector would be 5×10^{19} neutrons$\cdot m^{-2} \cdot s^{-1}$. With no oxide present, the same core could be operated at 270 MW to produce a peak unperturbed thermal neutron flux of almost 10^{20} neutrons$\cdot m^{-2} \cdot s^{-1}$.

Table 11. Reference core: thermal and flow parameters I

November 1985 reference design (calculation 25.4)[a]	
Active volume	35 L
Fuel	30 vol % (max) U_3Si_2
Clad	Aluminum alloy
Coolant	D_2O
Heated length	35 cm
Flow length	45 cm
Plate thickness	1.27 mm
Coolant gap	1.27 mm
Metal fraction	0.5

[a]Early version of reference core; fuel later changed to 35 vol % (max) U_3Si_2.

Table 12. Reference core: thermal and flow parameters II

Limiting criteria:

$\phi_{max} = \phi_{ib}$

$(t_{cl})_{plate\ max} = 354°C$

Coolant condition:

$P_o = 4.14$ MPa

$(\Delta t_{sub})_{o\ min} = 111°C$

"Clean" core:

q'''_{max} limited by ϕ_{ib} at $V < 42.7$ m/s

$q'''_{max} = 17.3$ MW/L at $V = 27.4$ m/s

Oxide core:

Assumed:

$\delta_{ox} = f\ (T_s,\ \theta)$ only

Moving hot spot halves the δ_{ox} calculated for a fixed hot spot

15-d core life

Calculated:

At $V = 15.24$ m/s and $\phi_{max} = 6.31$ MW/m^2, $(t_s)_{max} = 197°C$

For $\theta = 15$ d, $\delta_{ox} = 0.062/2 = 0.031$ mm

(q'''_{max}, V) pairs were computed that yield the same $(t_s)_{max}$

Values were chosen as the pair giving $(t_{fuel})_{max} = 354°C$

Result:

q'''_{max} limited by $(t_{cl})_{plate\ max}$

At $V = 27.4$ m/s, $q'''_{max} = 7.7$ MWt/L

Table 13. Reference core: thermal and flow parameters III

Case	With no oxide	With oxide[a]
Power, MW	270	135
$(\phi_n)_r$, 10^{19} neutrons/m^2s	10.0	5.0
V, m/s	27.4	27.4
P_o, MPa	4.14	4.14
P_i, MPa	5.57	5.57
ΔP_{syst}, MPa	2.30	2.30
q'''_{max}, MW/L	15.4	7.7
q'''_{avg}, MW/L	7.71	3.86
ϕ_{max}, MW/m^2	19.55	9.77
ϕ_{max}/ϕ_{ib}	0.90	0.45
t_{fuel}, max, °C	304	354
$t_{b,o}$, °C	91.7	70.6
Q_{core}, m^3/h	4935	4935
System pumping power (fluid kW)	3147	3147

[a]0.031-mm maximum.

5. CORROSION OF ALUMINUM FUEL PLATE CLADDING

J. C. Griess W. R. Gambill

5.1 Introduction

Aluminum alloy 6061 has provided an ideal cladding for the fuel plates in both the Advanced Test Reactor (ATR) and the HFIR and is the material of choice for cladding CNRR fuel plates. Both the ATR and HFIR operate at very high power densities, but the design power density for the CNRR is significantly greater still — higher than in any existing reactor. High power densities correspond to high heat fluxes across the fuel plate—water interface; this fact, combined with the formation of an adherent aluminum corrosion product on the fuel plate cladding, may limit the performance of the CNRR if aluminum-clad fuel plates are used.

5.2 Background Corrosion Information

Corrosion of aluminum in water leads to the formation of a low-conductivity layer of boehmite (α $Al_2O_3 \cdot H_2O$) that (1) increases the plate temperature (as much as 200°C in HFIR) and thereby reduces its structural strength, (2) increases fuel-plate to side-plate temperature difference, which causes thermal deflection, and (3) potentially increases the maximum fuel temperature beyond its allowable value. The mean thermal conductivity of the boehmite is low, only 2.25 W/m•K, which corresponds to an oxide temperature gradient of 444.7°C/mm per 1 MW/m^2 of heat flux. The maximum adherent oxide thickness appears to be about 0.05 mm. A favorable factor for the CNRR design is the experimental demonstration that decreasing the pH of pure H_2O or D_2O to 5.0 with nitric acid reduces the rate of oxide formation by a factor of about 2.7.

The corrosion rate of aluminum is limited by the oxide film that is slightly soluble in water. In quiet water that is saturated with corrosion product, the penetration of aluminum and the oxide thickness increase linearly with the square root of time (parabolic kinetics). In a flowing system where soluble aluminum is constantly removed from the water, oxide continues to dissolve and aluminum corrodes at a greater

rate than in a static system at the same temperature. With a heat flux across the corroding surface, the dissolution is enhanced because the temperature at the oxide-water interface is higher than the bulk water temperature, and the temperature and solubility gradients across the fluid film are greater the higher the heat flux. Under HFIR and ATR conditions about 70% of the aluminum that corrodes remains on the fuel plates. ORNL tests were conducted[26,27] during the early 1960s with H_2O at V = 7.6–15.2 m/s, t_b = 54–121°C, ϕ = 3.2–6.3 MW/m^2, and pH = 5.0–7.0. The ORNL data were correlated for pH = 5.0 by the expression:[26]

$$\delta_{ox} = 443\ \theta^{0.778} \exp\left(-4600/T_s\right) , \tag{5.1}$$

where

δ_{ox} = oxide thickness (mils),
θ = exposure time (h),
T_s = surface temperature (K).

A second correlation (of an unpublished data base)[28] was advanced one year later by the SRL:

$$\delta_{ox} = (8.109 \times 10^{-7})\phi\ \theta^{0.778} \exp\left(-1880/T_s\right) , \tag{5.2}$$

where

ϕ = heat flux (Btu/h•ft^2).

The two correlations for oxide thickness are in agreement only along the locus depicted in Fig. 21, in which subscripts 1 and 2 denote Eqs. (5.1) and (5.2), respectively.

In both correlations, the rate-determining temperature is that at the water-oxide interface. In view of the previous discussion, it is unlikely that the same correlation will be applicable without modification to the CNRR where both greater heat fluxes (13 vs 6.3 MW/m^2) and flow velocities (25 to 30 vs 15 m/s) will prevail. The higher heat flux will result in a higher temperature at the oxide-solution boundary, a fact that causes a greater rate of oxide formation. On the other hand, the higher flow velocity reduces the surface temperature and the stationary

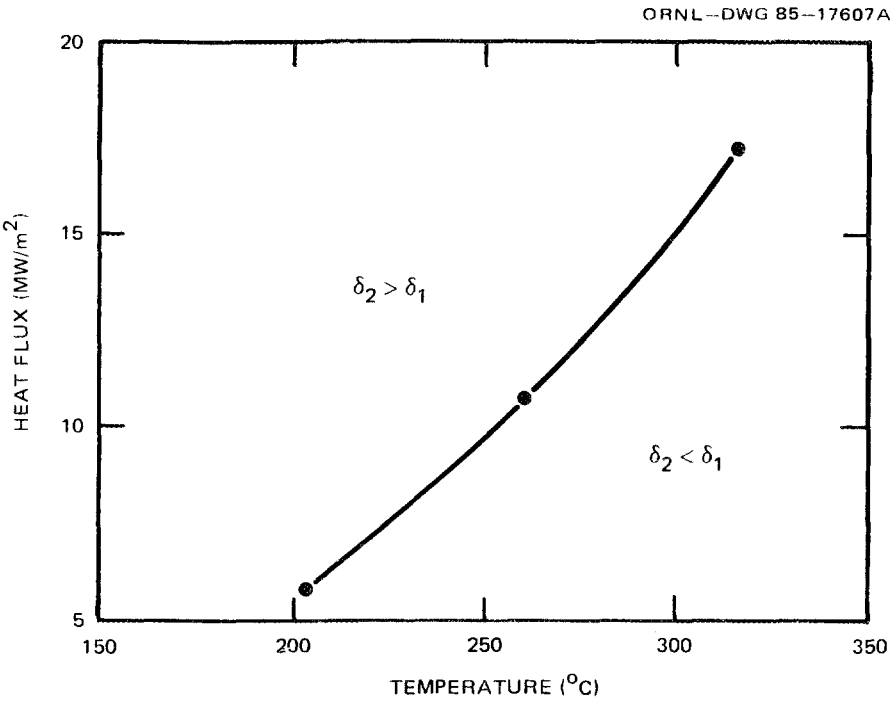

Fig. 21. Comparison of two oxide-thickness correlations.

fluid film thickness, both of which should tend to reduce the rate of oxide growth on the aluminum surfaces. How these and other factors interact to produce an oxide film under CNRR conditions cannot be predicted confidently from the data in hand. Therefore, an experimental program is required to establish whether an aluminum alloy cladding can be used under the conditions currently anticipated in the CNRR core.

5.3 Test Plan

In view of the foregoing discussion, useful corrosion data can only be obtained under conditions of temperature, velocity, heat flux, and water chemistry that approximate those expected in the CNRR. Consequently, a recirculating test loop will be constructed that has bypass demineralization capability and in which aluminum specimens can be tested with heat fluxes up to 16 MW/m^2 across the interface and with coolant velocities up to 30 m/s. In this facility, a correlation between temperature and oxide-formation rate will be developed for much higher heat fluxes and flow velocities than have been previously examined.

The first tests will be with 6061 aluminum, the same alloy used for cladding the fuel in the HFIR and ATR. If the untreated alloy appears to be unsuitable, surface modification including ion implanting and plating as well as the use of different, perhaps more highly alloyed, aluminum alloys will be examined. The effect of additives to the coolant may also be explored. Note that the CNRR will use D_2O as the primary coolant, whereas both the ATR and HFIR use H_2O. Although no significant difference in corrosion of aluminum is expected in the two coolants, some of the tests will be conducted with D_2O.

If aluminum alloys prove unacceptable under the design conditions, two alternatives exist: restrict the performance of the CNRR to the level where aluminum can be used or use a cladding material that is more resistant to corrosion than aluminum. Neither alternative is attractive. Reducing the power density of the reactor will reduce the neutron flux available for the experimenters. Selection of an alternate cladding material such as stainless steel or Zircaloy will essentially eliminate the corrosion problem but will greatly increase the cost of fuel fabrication and reprocessing. It has been crudely estimated that if the relative cost of an aluminum clad core is 1, then stainless steel would be about 5 and Zircaloy about 10. Furthermore, both materials have a much lower thermal conductivity than aluminum, a fact that would require thinner cladding than with aluminum and probably present fabrication problems.

5.4 Summary

An aluminum alloy is the most desirable cladding material for fuel plates in high-performance reactors that have low-temperature coolant. The use of aluminum cladding in such reactors is limited primarily by the formation of a poorly conducting oxide layer on the cladding surface. An aluminum alloy, 6061, has been highly successful as a cladding for both HFIR and ATR fuel plates, but because of the significantly higher heat fluxes expected to exist across the cladding of the CNRR fuel plates, the use of untreated aluminum cladding is questionable. Therefore, a test loop will be built that can operate under flow and heat transfer conditions expected in the CNRR to determine under what conditions an aluminum alloy can be used to clad CNRR fuel plates.

6. FUEL MATERIALS

G. L. Copeland

To obtain the desired flux levels for the CNR along with a reasonable core lifetime, a higher specific uranium density will be required than is currently achievable with the fuel materials now being routinely used in research reactors (UAl_x and U_3O_8). Fortunately, just such a high density fuel has been developed and is now being tested through the Reduced Enrichment Research and Test Reactor (RERTR) Program being conducted for DOE by the Argonne National Laboratory (ANL). This fuel is U_3Si_2 dispersed in aluminum and clad with aluminum alloy just like the currently used compounds.[29] Of course, the goal of the RERTR program is to decrease the U-235 enrichment but to increase the total uranium loading of the fuel to maintain reactor performance. When U_3Si_2 is used with highly enriched uranium, it will offer a specific U-235 loading of 2 to 3 times that possible with the current compounds. The new fuel has been proven to be stable at high volume fractions to essentially full burnup with 20% enriched uranium. Miniature test plates and full-size elements have been tested in the Oak Ridge Research Reactor (ORR)[30] and some foreign reactors in the RERTR Program. The ORR is now being phased into a full core of the low-enriched silicide fuel. In addition, miniplates are being tested in the ORR containing fully enriched U_3Si_2 at lower volume fractions.

It will remain for the CNR program to test and demonstrate the performance of the silicide fuel at the heat flux and burnup conditions expected in the CNRR. Figure 22 shows the conditions at which experiments have been performed and also shows the expected burnup variation in the CNRR fuel. Based on current results, the CNRR design appears to be a reasonable extrapolation with a high probability of success. Additional development that appears to be needed to optimize performance is axial grading of the fuel at the plate ends in addition to the radial grading now used in HFIR. This again appears to be a reasonable extension of existing technology.

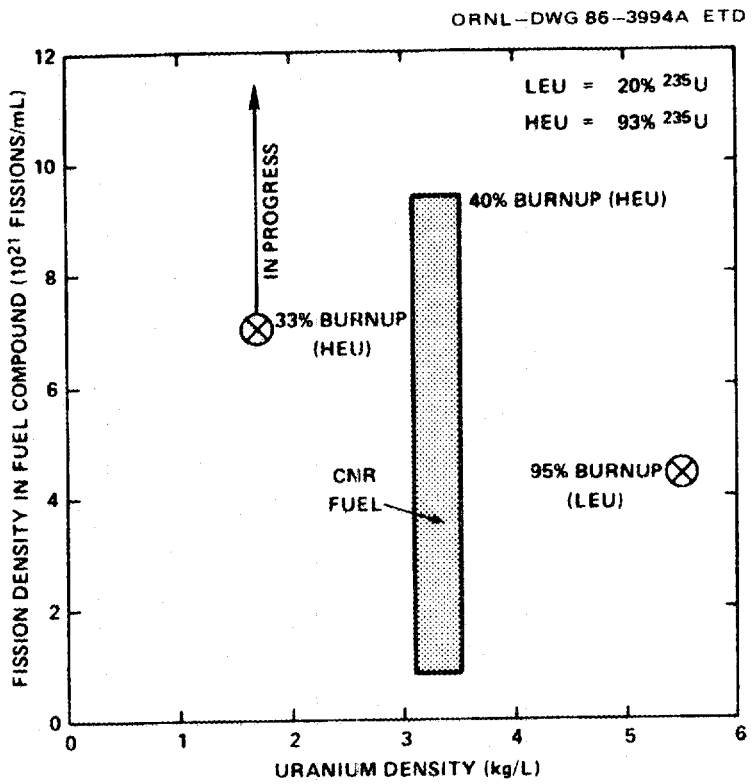

Fig. 22. Currently available silicide fuel irradiation data and expected CNR operating limits.

7. COLD SOURCE FEASIBILITY STUDY

I. I. Siman-Tov R. T. Primm III

Based on a survey of cold neutron sources (CNSs) in operation and under design, it was concluded that the well-established CNSs and associated technologies are those using liquid hydrogen (LH) or liquid deuterium (LD). The feasibility of a CNS similar to the vertical one in operation at the ILL for the CNR must be determined. Consideration will be given to using a combination of LH and LD or moderating the neutrons in more than one stage using more than one moderating material. These options may have to be considered if the geometry, safety, or economy of operation with LD alone appears unsatisfactory. It is possible that the CNR staff could use the ILL refrigeration system to run tests on the CNR CNS design if necessary. Table 14 lists primary parameters to be evaluated for the CNR CNS to achieve the desired cold flux of 2 to 3 × 10^{19} neutrons$\cdot m^{-2} \cdot s^{-1}$ (Refs. 31–34).

7.1 Cold Neutron Scattering Cross Sections

To size the CNR CNS properly, scattering cross sections for cold (~20 K) liquid deuterium and liquid hydrogen are needed. A paper describing a theoretical derivation of the scattering kernels was written by Young and Koppel.[35] M. W. Waddell encoded these equations and generated the scattering kernels. N. M. Greene wrote a computer program to convert the generated data to Evaluated Nuclear Data File 6 format. Greene then generated three cross-section sets [parahydrogen, orthohydrogen (LH having two spin states), and deuterium] in a 51-energy-group structure with the upscatters collapsed out. Upscatter cross sections were removed to be compatible with other 51-group data — Zr, Mg, O, 293 K H, and 293 K D — which were added to the three cold cross-section sets by L. R. Williams to generate a cold source problem library.

7.2 Computational Studies of the CNR Cold Source

A calculational study has begun to determine the appropriate diameter for a spherical cold source. The initial step in this study was to

Table 14. Comparison of ILL and CNR cold sources[a]

Item	ILL-Vertical cold source	CNR — proposed cold source
Unperturbed thermal flux at nose of beam tube	2.2E18 neutrons•m^{-2}•s^{-1} (original design) 3.3E18 to 4.0E18 neutrons•m^{-2}•s^{-1} (present design) (Ref. 31)	2 to 3E19 neutrons•m^{-2}•s^{-1}
Gain factors	30 at 6Å; 60 at 10Å (calculated) (Ref. 31) 70 at 10Å (experimental) (Ref. 32)	Minimum — same as ILL (?)
Position in reflector	70 cm from core axis (Ref. 33)	Constraints: distance of required thermal flux from closest structural barrier (reactor vessel or other structure)
Shape and size	Sphere of 38-cm diam (Ref. 33)	Similar shape and size to be determined (other options — cylinder, disk)
Heat to be removed to maintain LD_2 at 25 K	5 kW (Ref. 33)	To be determined
Heat sources and relative strength	Vessel (W) / LD_2[a] (W) / Total (W) Neutrons: 190 / 190 Primary gamma: 431 / 896 / 1327 Gamma capture: 639 / 828 / 1467 Beta capture: 1127 / 1127 Syphon chimney: 387 Total: 2197 / 1914 / 4498 (Ref. 34)	To be determined; strength is a function of CNS position in reflector, size, materials, and configuration
Heat removal mechanism	D_2 boiling (20% void fraction) — thermosyphon circulates 15 g/s D_2 (Ref. 33)	Same cooling method Constraint: limited by void fraction (up to 20% void fraction may be acceptable)
Refrigeration system	Helium refrigeration 360 kW needed to remove 5 kW (Ref. 33)	Constraint: limited by available equipment

[a]LD_2 = liquid deuterium; molecular form is D_2.

calculate the angular fluxes at the point in the reflector where the peak thermal flux occurs. This was accomplished by using the one-dimensional (1-D) discrete ordinates theory code, XSDRNPM, and creating a spherical model of the CNRR and reflector. Cross sections were supplied from a 27-group library derived from the Evaluated Nuclear Data File — Version V and processed according to the procedure described in Sect. 3 except that no spectral (energy) weighting was performed.

A spherical model of the reactor core was utilized so that the angular flux source term could be input directly into a second, spherical, cold source model rather than having to convert fluxes from cylindrical to spherical geometry. Considering the approximations inherent in a 1-D calculation, the spherical core approximation is not believed to introduce a significant error.

The calculated (S4 quadrature) angular fluxes at the point of maximum thermal flux were used as a shell source in a second ANISN model (see Fig. 23). The same angular quadrature was used as was in the core model. The thickness of the reflector D_2O region in the second ANISN model varied from case to case but was ~20 cm.

The reflector D_2O region was included in the second ANISN model so that feedback effects of the cold source on the surrounding D_2O reflector could be examined. Two containment metals, aluminum and magnesium, were examined; two cold materials, LD and LH, were investigated.

The source spectra for the unperturbed D_2O reflector and for the central position of each of the two cold materials (magnesium metal container) are plotted in Fig. 24. The radius of the cold region was rather arbitrarily assumed to be 400 mm. The LH was assumed to be composed of 50% parahydrogen and 50% orthohydrogen.

The cold D source yields a more thermalized neutron source than the cold H source. In addition, with LD, the absolute value of the flux in the most thermal group at the center point is two orders of magnitude higher than the value when LH is utilized. This is believed to be caused by the higher thermal absorption of hydrogen and the large cold source diameter. For both moderating materials, the use of magnesium rather than aluminum for the vessel wall results in a higher flux inside the

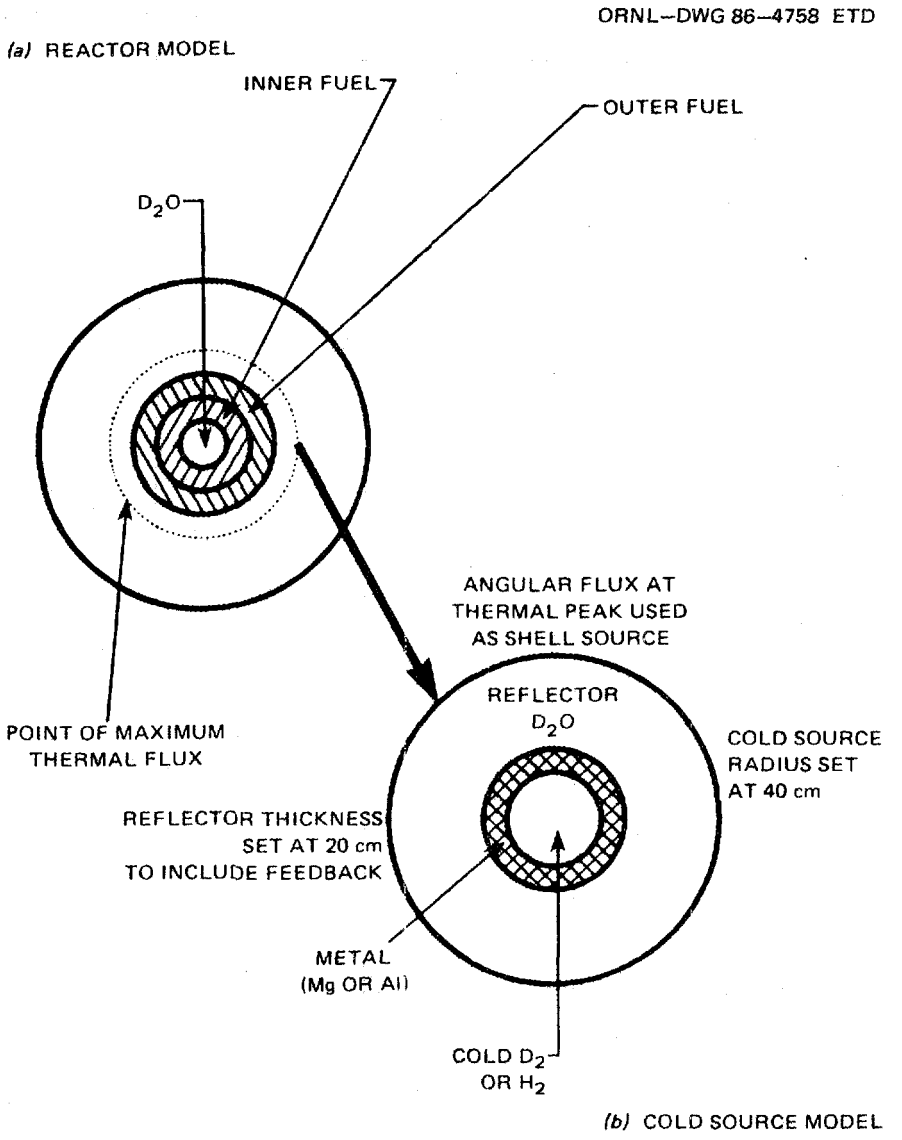

Fig. 23. Computer models used to investigate cold source.

cold source. The thickness of the vessel wall was assumed to be 1.5 mm in all cases.

The unusually high fast flux fraction in the LH calculation seems to be due to the larger thermal absorption of hydrogen relative to deuterium and to the fact that the areas under the curves are normalized to 1.0. The absolute value of the flux in the fastest group in the hydrogen calculation is essentially the same as that in the deuterium calculation.

ORNL–DWG 86–4759 ETD

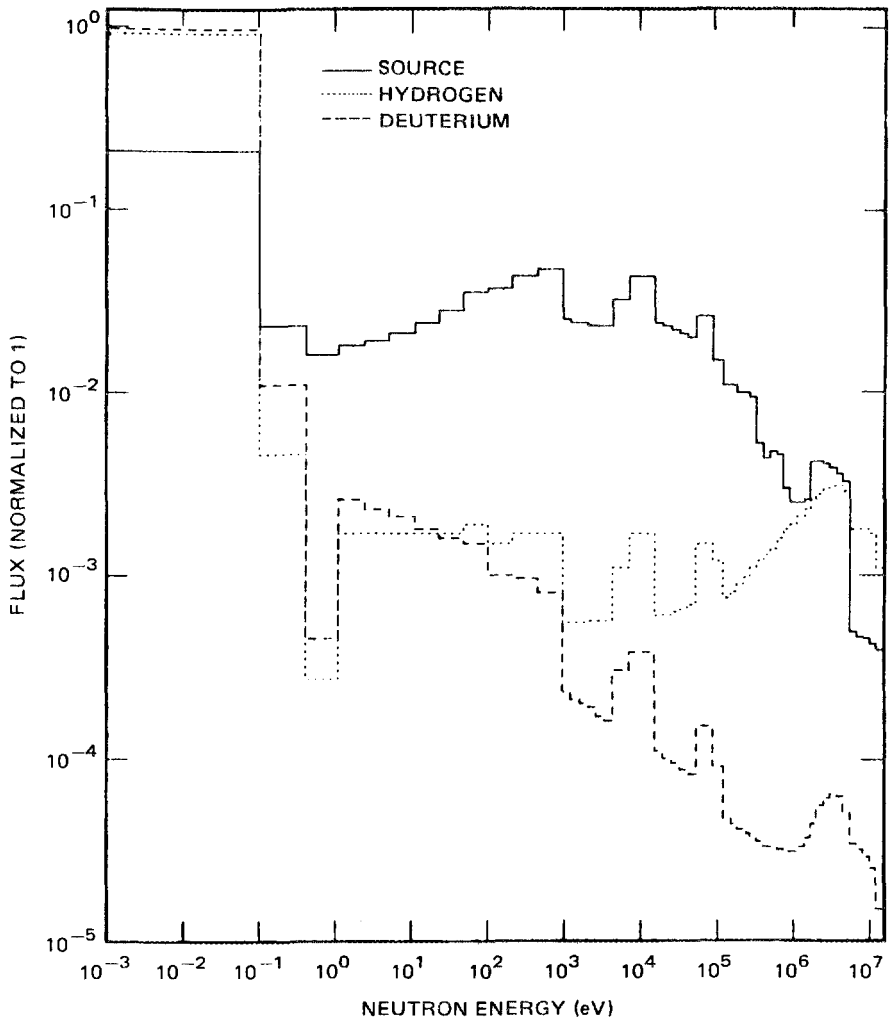

Fig. 24. Neutron spectra at center of cold source.

The increase in the thermal group by only a factor of 5 for the cold sources relative to the unperturbed D_2O reflector source reveals that an inappropriate group structure has been chosen. As was shown in Table 14, the design goal is to have a gain in neutron flux of 70 at an energy of 10 Å (0.8 meV). To evaluate whether the CNR CNS can achieve this criterion, a new energy group structure with many more groups below 0.1 eV is needed. Likewise, it would seem prudent to ensure that upscatter matrices are generated in the new library.

7.3 Revised Thermal Energy Group Structure

It can be shown that the energy distribution of cold neutrons (number per unit energy) is given by Eq. (7.1):

$$f(E) = \frac{E}{E_o^2} (e^{-E/E_o}) , \tag{7.1}$$

where E_o (in meV) is equal to 0.0616 × temperature (K), and the entire distribution is normalized such that

$$\int_0^\infty f(E)\ dE = 1 .$$

The value of the function f(E) at various energies for neutrons in thermal equilibrium with a 20 K cold source is given in Table 15. The full width at half maximum is seen to be about 4.5 meV.

To obtain more information regarding the degree of thermalization provided by cold sources of various sizes, the judgment was made that the most thermal group of the 51-group library should be subdivided into ten

Table 15. Distribution function for neutrons in thermal equilibrium with a cold source at 20 K

Energy (meV)	f(E) (No./meV)	Energy (meV)	f(E) (No./meV)
0.05	0.0163	2.7	0.1898
0.1	0.0318	3.0	0.1772
0.4	0.1068	3.5	0.1546
0.7	0.1570	4.0	0.1322
1.0	0.1884	5.0	0.0925
1.3	0.2059	7.0	0.0406
1.7	0.2135	10.0	0.0102
2.0	0.2110	15.0	0.0008
2.3	0.2039		

energy groups. Using 0.01 meV as a starting energy, Eq. (7.1) was integrated to determine 10 intervals, each of which would contain ~10% of the neutrons present in a 20 K cold source. The energy boundaries are shown in Table 16. The number of fast groups in the new library could be reduced to compensate for the increased computer running time that will result from the greater number of thermal groups.

Table 16. Thermal energy boundaries for future cold source calculations

Group No.	Energy boundaries (meV)
1	0.01–0.55
2	0.55–0.85
3	0.85–1.15
4	1.15–1.45
5	1.45–1.80
6	1.80–2.15
7	2.15–2.60
8	2.60–3.25
9	3.25–4.45
10	4.45–100.0

8. PROGRAM PLAN

R. T. Primm III

A plan describing the experiments and development tests that must be conducted to support the CNR design was drafted by Primm and Barthold. Data were gathered from several individuals within the Martin Marietta Energy Systems organization. The plan includes identification of problem areas, justification for proposed experiments or tests, description of the proposed activities, and estimates of costs and schedules. Several revisions were made to the original draft, and the final draft is in publication.

A summary of the costs of the experiments and analyses is provided in Table 17. A tentative program schedule is shown in Fig. 25.

Table 17. Financial plan for CNR experiments and development tests

Task		Cost (1986 $ in thousands)				
No.	Description	Year 1	Year 2	Year 3	Year 4	Year 5
	Management	210	250	250	250	250
1	Silicide fuel	525	1,150	3,050	1,000	
2	Aluminum corrosion	575	500	550	550	
3	Thermal-hydraulics	360	610	460		
4	Control elements	65	190	720		
5	Critical experiments	100	190	250	1,130	625
6	Structural tests		1,100	3,630	1,930	
7	Cold source	110	965	3,315	1,000	
8	Hot source	50[a]				
9	Shielding	50[a]				
10	Design and safety	455	1,800	2,600	750	
	Other[b]		445	275	2,290	2,825
	Total	2,500	7,200	15,100	8,900	3,700

[a]Money to be used to define plans and cost for carrying out this part of the program.

[b]Contingency for costs to be identified in Tasks 8 and 9 and also to provide funding for final core analyses.

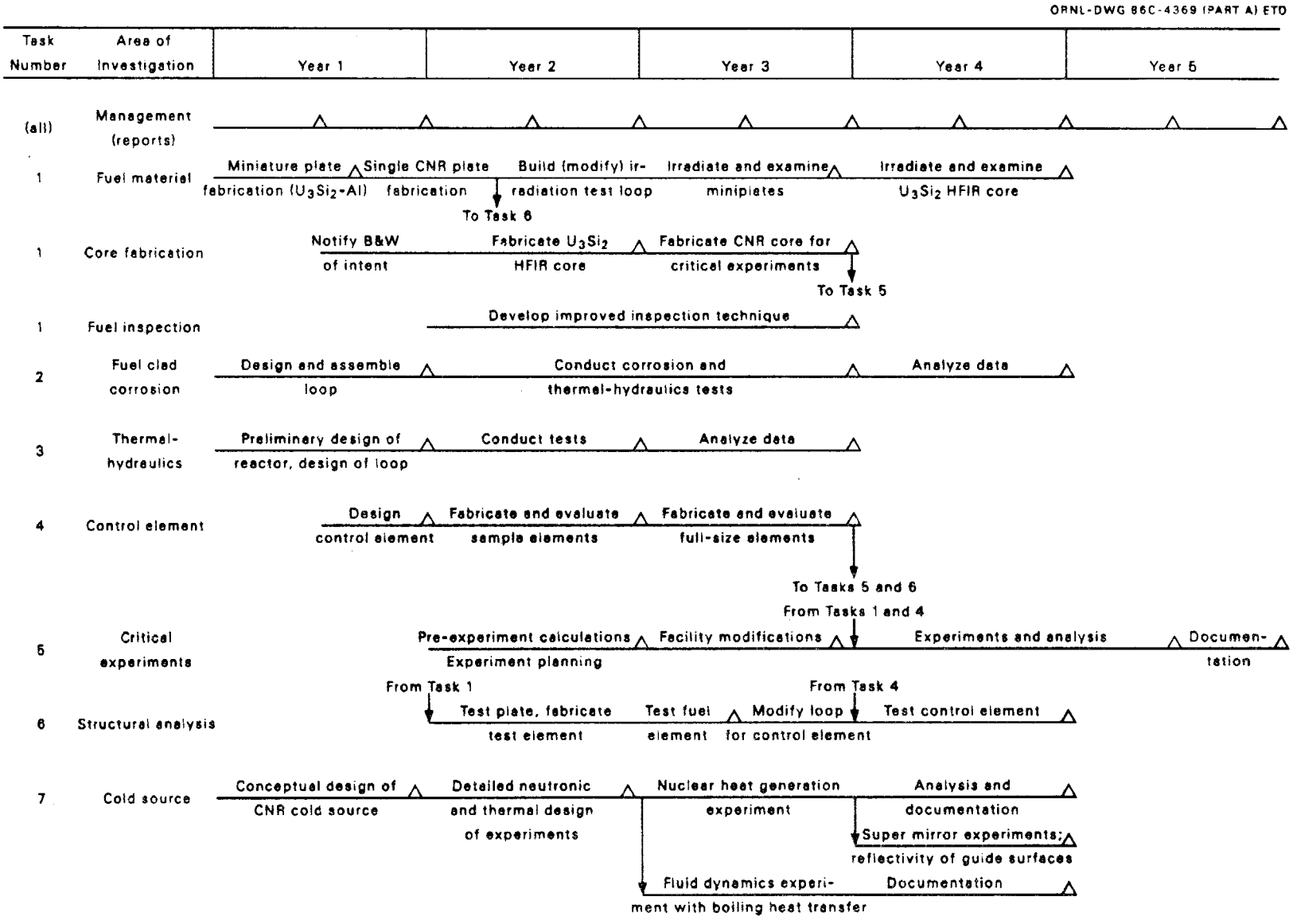

Fig. 25. CNR program schedule.

ORNL-DWG 86C-4369 (PART B) ETD

Task Number	Area of Investigation	Year 1	Year 2	Year 3	Year 4	Year 5
8	Hot source	Assessment of size and scope of task				
9	Shielding	Assessment of size and scope of task				
10	Safety	Assessment of tritium handling system; identification of accidents	Collection of failure rate data	Begin PSAR	Complete PSAR	
10	Balance of plant (A/E)	A/E selection criteria document; Select A/E	Begin conceptual design	Complete conceptual design		
10	Environmental studies	Action description memo	Issue environmental assessment	Issue environmental impact statement		

Fig. 25 (continued)

REFERENCES

1. *Major Facilities for Materials Research and Related Disciplines*, comp. Major Materials Facilities Committee, Commission on Physical Sciences, Mathematics, and Resources, National Research Council, July 24, 1984.

2. R. M. Moon, ed., *Proceedings of the Workshop on Instrumentation for the Advanced High-Flux Reactor*, CONF-8405192, Oak Ridge Natl. Lab., May 30, 1984.

3. G. H. Lander and V. J. Emery, *Scientific Opportunities with Advanced Facilities for Neutron Scattering*, CONF-8410256, Argonne Natl. Lab., 1985.

4. F. C. Difilippo et al., "A Preliminary Reactor Design for the Center for Neutron Research," *Nuclear Instruments and Methods in Physics Research* (in press).

5. R. M. Moon, ed., *Proceedings of the Workshop on Instrumentation for the Advanced High-Flux Reactor*, May 1984, CONF-8405192.

6. F. Mezei, *Comm. on Physics* 1, 81 (1976).

7. P. Ageron, private communication to R. M. Moon, Oak Ridge National Laboratory.

8. H. Maier-Leibnitz and T. Springer, *Reactor Science and Technology* 17, 217 (1963).

9. C. V. Parks et al., *SCALE: A Modular Code System for Performing Standardized Computer Analyses for Licensing Evaluation*, NUREG/CR-0200, Vol. 3 (ORNL/NUREG/CSD-2), Martin Marietta Energy Systems, Inc., Oak Ridge Natl. Lab., December 1984.

10. D. Garber, C. Dunford, and S. Pearlstein, *ENDF-102 Data Formats and Procedures for the Evaluated Nuclear Data File, ENDF*, BNL-NCS-50496, Brookhaven Natl. Lab., March 1976.

11. D. R. Vondy, T. B. Fowler, and G. W. Cunningham III, *The Bold Venture Computation System for Nuclear Reactor Core Analysis, Version III*, ORNL-5711, Union Carbide Corp. Nuclear Div., Oak Ridge Natl. Lab., June 1981.

12. Personal communication from R. D. Cheverton, Oak Ridge National Laboratory, to R. T. Primm III, Oak Ridge National Laboratory, September 1984.

13. B. S. Petukhov, "Heat Transfer and Friction in Turbulent Pipe Flow with Variable Physical Properties," in *Advances in Heat Transfer*, Academic Press, New York, 6, 503 (1970).

14. H. Hausen, *Heat Transfer in Counterflow, Parallel Flow and Cross Flow*, McGraw-Hill, New York, 1983, p. 31.

15. J. L. Crandall, comp., *The Savannah River High Flux Demonstration*, SRL Report DP-999, 1965.

16. D. R. Miller, *Critical Flow Velocities for Collapse of Reactor Parallel Plate Fuel Assemblies*, KAPL Report KAPL-M-DRM-13, 1958.

17. R. L. Webb, "A Critical Evaluation of Analytical Solutions and Reynolds Analogy Equations for Turbulent Heat and Mass Transfer in Smooth Tubes," *Wärme-und Stoffübertragung* [*Thermo- and Fluid Dynamics*] 4, 197 (1971).

18. F. C. Difilippo et al., "A Preliminary Reactor Design for the Center for Neutron Research," *Nuclear Instruments and Methods in Physics Research* (in press), p. 120.

19. A. E. Bergles and W. M. Rohsenow, "Effects of Heat Flux on the Corrosion of Aluminum by Water, Part IV. Tests Relative to the Advanced Test Reactor and Correlation with Previous Results," *J. Heat Transfer* 86, 365 (1964).

20. E. J. Davis and G. H. Anderson, "Evaluation of Mark 22 Cladding," *A.I.Ch.E. Journal* 12(4), 774 (1966).

21. W. R. Gambill, "The Determination of Forced Convection Surface-Boiling Heat Transfer," *Chemical Engineering Progress Symposium Series* 59(41), 71 (1963).

22. S. S. Kutateladze and A. I. Leont'ev, "The Incipience of Nucleate Boiling in Forced Convection Flow," *Proceedings of Third International Heat Transfer Conference* III, 1, 1966.

23. D. H. Knoebel et al., *Generalized Prediction of Burnout Heat Flux for Flowing, Subcooled, Wetting Liquids*, SRL Report DP-1306, 1973.

24. W. R. Gambill, *Design Curves for Burnout Heat Flux in Forced-Convection Subcooled Light-Water Systems*, ORNL/TM-2421, Union Carbide Corp. Nuclear Div., Oak Ridge Natl. Lab., 1968.

25. H. A. McLain, *HFIR Fuel Element Steady State Heat Transfer Analysis, Revised Version*, ORNL/TM-1904, Union Carbide Corp. Nuclear Div., Oak Ridge Natl. Lab., 1967.

26. J. C. Griess, H. C. Savage, and J. L. English, *Effect of Heat Flux on the Corrosion of Aluminum by Water. Part IV. Tests Relative to the Advanced Test Reactor and Correlation with Previous Results*, ORNL-3541, Union Carbide Corp. Nuclear Div., Oak Ridge Natl. Lab., February 1964.

27. V. A. Walker, M. J. Graber, and G. W. Gibson, *ATR Fuel Materials Development Irradiation Results — Part II*, Idaho National Engineering Laboratory, 100-17157, June 1966.

28. R. S. Ondrejcin, Savannah River Lab. Memorandum DPST-83-324, "Evaluation of Mark 22 Cladding," 11, 1983.

29. "Post-Irradiation Analysis of Experimental Uranium Silicide Dispersion Fuel Plates," *Proceedings of the 1984 International Meeting on Reduced Enrichment for Research and Test Reactors, Argonne, IL, October 15–18, 1984*, ANL/RERTR/TM-6, July 1985.

30. J. L. Snelgrove et al., "The Whole Core LEU Fuel Demonstration in the ORR," *Proceedings of International Meeting on Reduced Enrichment for Research and Test Reactors, Petten, The Netherlands, October 14–16, 1985*, March 1986.

31. P. Ageron and W. Marupe, "ILL Facilities for Fundamental Physics Experiments," *Journal de Physique*, Colloque C3, supp. au no 3, Tome 45, March 1984.

32. P. Ageron, *Special Neutron Sources*, IAEA CN 46/016.

33. J. Verdier, J. M. Astruc, and P. Ageron, "Source Froide du Reacteur attaut Flux de Li Institut Laue-Langevin," *Bull. d'Inform. Sci. et Tech.* No. 215, June 1976.

34. P. Ageron, Tabulated information from the December 1985 Workshop on an Advanced Steady-State Neutron Facility, National Bureau of Standards, Gaithersburg, Md.

35. J. A. Young and J. U. Koppel, "Slow Neutron Scattering by Molecular Hydrogen and Deuterium," *Physical Review* 135(3A), A603–611 (August 1964).

Internal Distribution

1. T. D. Anderson
2. S. J. Ball
3. D. E. Bartine
4. E. E. Bloom
5. T. E. Cole
6. G. L. Copeland
7. W. G. Craddick
8. F. C. Difilippo
9. W. R. Gambill
10. J. A. Getsi
11. J. C. Griess
12. R. M. Harrington
13. L. Horton
14. O. L. Keller
15. D. B. Lloyd
16. P. E. Melroy
17. B. H. Montgomery
18. R. M. Moon
19. J. A. Murray
20. F. R. Mynatt
21. R. E. Pawel
22. F. J. Peretz
23-27. R. T. Primm III
28. J. H. Swanks
29. I. I. Siman-Tov
30. P. B. Thompson
31. K. R. Thoms
32. H. E. Trammell
33. R. E. Uhrig
34. C. D. West
35-90. M. K. Wilkinson
91. R. G. Wymer
92. G. T. Yahr
93. A. Zucker
94. ORNL Patent Office
95. Central Research Library
96. Document Reference Section
97-98. Laboratory Records Department
99. Laboratory Records (RC)

External Distribution

100. P. Ageron, Institute Laue Lagevin, 156X 38042, Grenoble Cedex, France
101. W. P. Barthold, Barthold & Associates, Inc., P.O. Box 11730, Albuquerque, NM 87192
102. G. Bauer, KFA Julich, SNQ, P.O. Box 1913, D15170 Julich, West Germany
103. W. Gläsek, Fakultät für Physik, Technische Universität München, D-8046 Garching, West Germany
104. K. J. Henry, Head, Research Reactors Division, AERE Harwell, Oxfordshire, OX11 ORA, England
105. Masashi Iizumi, Japan Atomic Energy Research Institute; 222, Uchisaiwai-cho; Chiyoda-ku, Tokyo, Japan
106. Nobuhiki Kunitomi, Osaka University, 1-1 Yamadaoka, Fuita-Shi, Osaka 565 Japan
107. J. A. Lake, Nuclear Engineering, Idaho National Engineering Laboratory, P.O. Box 1625, Idaho Falls, ID 83415
108. L. LeSage, Argonne National Laboratory, 9700 South Cass Ave., Argonne, IL 60439
109. A. Olsen, Argonne National Laboratory, 9700 South Cass Ave., Argonne, IL 60439
110. J. R. Powell, Brookhaven National Laboratory, Upton, NY 11973
111. John J. Rush, National Bureau of Standards, Washington, D.C. 20234

112. J. L. Snelgrove, Coordinator, Engineering Applications, RERTR Program, Argonne National Laboratory, 9700 South Cass Ave., Argonne, IL 60439
113. Peter von der Hardt, Head, HFR Division, Joint Research Center, Petten Establishment, Postbus 2, 1755 ZG Petten, The Netherlands
114. Y. Yamada, University of Tokyo, Hongo, Bunkyo-ku, Tokyo, Japan
115. Office of Assistant Manager for Energy Research and Development, Department of Energy, ORO, Oak Ridge, TN 37831
116-142. Technical Information Center, Department of Energy, Oak Ridge, TN 37831